Pergamon

Geochimica et Cosmochimica Acta, Vol. 67, No. 11, pp. 2043–2062, 2003

0016-7037/03 $30.00 + .00

doi:10.1016/S0016-7037(02)01340-6

Lattice diffusion of Ar in quartz, with constraints on Ar solubility and evidence of nanopores

E. B. WATSON* and D. J. CHERNIAK

Department of Earth and Environmental Sciences, Rensselaer Polytechnic Institute, Troy, NY 12180, USA

(*Received January* 30, 2002; *accepted in revised form November* 15, 2002)

Abstract—Diffusion and solubility of Ar in optically clear natural and synthetic quartz crystals were examined at ~500 to 1200 °C by treating polished specimens in pressurized Ar (1–185 MPa) and characterizing the resulting diffusive-uptake (or subsequent diffusive-loss) profiles using Rutherford backscattering spectroscopy (RBS). Analytical uncertainty leads to significant scatter in the data, but the Ar diffusivity, D, is reasonably well constrained by the following Arrhenius relationship:

$$D = 8.2^{+8.8}_{-4.2} \times 10^{-19} \exp[(-6150 \pm 750)/T(K)]\ m^2/s$$

No effects of crystallographic orientation or quartz structural form (α or β) are discernible.

Apparent solubilities typically fall between 1000 and 3000 ppm (by mass), with large uncertainties ($\pm 50-60\%\ 2\sigma$), but some lower values (~700 ppm) are observed near the low end of the Ar pressure range investigated. Occasional high-concentration outlier values fall between 5000 ppm and 3.8 wt.% Ar. These do not correlate with Ar pressure, suggesting extrinsic (non-lattice) siting of Ar in some cases. Field-emission SEM images and numerical simulations of the diffusion process document isolated nanopores as the hosts for the occasional very high concentrations of Ar (observable pores range down to ~10 nm in diameter; indirect evidence points to smaller ones as the more common sinks for Ar). The systematics of the data suggest an actual (lattice) solubility of ~2000 ppm at 100- to 200-MPa Ar pressure, which is equivalent to a partition coefficient of $\sim 0.001 cm^3 STP/g \cdot atm$. Using either organic clathrate or fullerene as the Ar sources, 1-GPa experiments in a piston-cylinder apparatus result in similar uptake of Ar into quartz, in this case through partitioning equilibrium with C-O-H fluid (clathrate source) or amorphous carbon (fullerene source).

The ability of quartz, relative to other minerals, to incorporate significant amounts of Ar may allow this ubiquitous and abundant mineral to serve as a local sink for Ar in crustal rocks lacking a free fluid phase. The diffusion data permit open-system behavior of Ar in quartz below the closure temperature of biotite and other ^{40}Ar source minerals.

1. INTRODUCTION

As a noble gas produced mainly by decay of an abundant, long-lived radionuclide, argon is of central importance to geochronology and to models of terrestrial degassing. Much is known about the behavior of Ar in natural systems, but there do remain gaps in our understanding of its solid-Earth geochemistry. Attention has been focused, logically, on potassic minerals such as K-feldspars, micas, and amphiboles, because these are the immediate hosts of radiogenic ^{40}Ar. The Ar diffusion characteristics of these minerals have been of particular interest, because these largely determine the intragrain Ar retentivity in geologic settings (see information summarized in McDougall and Harrison, 1999). Remaining questions include the source and acquisition mechanism of excess radiogenic Ar in minerals (see, e.g., Foland, 1979; Roddick et al., 1980; Harrison and McDougall, 1981; Cumbest et al., 1994; Scaillet, 1996; Kelley and Wartho, 2000; Baxter et al., 2002), the pathway and efficiency of crust-atmosphere equilibration (see, e.g., Roddick et al., 1980; Cumbest et al., 1994) and the existence and role of local sink minerals that do not themselves generate ^{40}Ar (Baxter et al., 2002).

As a first step in exploring some of the unknowns noted above, we undertook a study of the diffusion and solubility behavior of Ar in quartz. This ubiquitous and abundant mineral is commonly associated with potassic minerals in the crust and is thus a potential sink for ^{40}Ar. Our study is preceded by the work of Roselieb et al. (1997) who examined the diffusive uptake and loss of Ar in quartz powders using bulk degassing techniques combined with electron microprobe and SEM observations. We, in contrast, examined Ar diffusion in large single crystals and directly characterized Ar diffusive-uptake profiles in the near-surface region using Rutherford backscattering spectroscopy (RBS). The method enables us not only to obtain a diffusivity, but also to gain some insight into the solubility of Ar in the quartz lattice.

This study is the first of a series of investigations of noble-gas behavior in minerals using direct depth-profiling techniques. There is strong motivation to examine other gases and other minerals, but in most cases the technique-development aspects are proceeding slowly. Argon in quartz constitutes a relatively heavy element (Ar) in a much lighter matrix (Si+O) that is nominally free of impurities near mass 40; given sufficiently high Ar solubility, the system is accessible using well-established RBS techniques.

2. MATERIAL AND METHODS

2.1. Overview

The simple strategy of this study is to subject polished quartz specimens to pressurized Ar at high temperatures, causing Ar to diffuse into the near-surface region. Argon-uptake profiles in the quenched

* Author to whom correspondence should be addressed (watsoe@rpi.edu).

specimens were then characterized by RBS, and from them diffusivities were obtained by fitting the profiles to a standard diffusion model. In experiments such as these, the diffusant concentration decreases monotonically as a function of distance from the specimen surface, but in principle, the concentration at the surface represents the diffusant solubility at run conditions—in this case of Ar in the quartz lattice. Most of our Ar-uptake experiments were procedurally similar to those of Roselieb et al. (1997) and also to those of Carroll and Stolper (1991) addressing Ar diffusion and solubility in silica glass.

Eleven experiments were performed using sources of Ar other than nearly pure pressurized gas. As a prelude to this study, we developed two methods of synthesizing Ar-bearing compounds that are stable at atmospheric conditions, so we were able to introduce Ar into experimental containers in powder form. One of the compounds was hydroquinone (dihydroxybenzene; $C_6H_4[OH]_2$), which forms stable noble-gas clathrates when crystallized under pressurized gas (Greenwood and Earnshaw, 1984). We were also successful in "argonating" fullerenes at modest Ar pressures, which release some of their Ar to quartz at high temperatures and pressures.

2.2. Materials and Experiment Details

2.2.1. Quartz crystals and preparation procedures

Two types of quartz were used in this study: natural "rock crystal" (Arkansas, USA) obtained from Ward's Natural Science Establishment and a large (~20 cm) synthetic crystal grown commercially for use in electronic oscillators. Both are optically clear overall, but both also contain localized patches and trails of fluid inclusions visible with an optical microscope. The crystals were cut with a low-speed diamond saw into ~1-mm-thick slabs oriented either perpendicular or parallel to the *c* crystallographic axis. Every effort was made to avoid fluid inclusions, but this was found to be impossible because the inclusions range down to 10 to 20 nm or less in size (see section 3.2). The cut slabs were ground to overall flatness with SiC or diamond and polished with 1-μm alumina followed by colloidal silica. Final working-size specimens (~3 × 3 × 1 mm) were obtained by cutting the polished slabs with a diamond saw or by scoring and breaking them.

Both the natural and synthetic quartz crystals were grown under hydrothermal conditions, and it was anticipated that the initial presence of hydrous species dissolved in the quartz lattice might influence Ar diffusion and/or solubility. For this reason, most of the quartz specimens used in this study were preannealed in air at 1000 °C for 3 to 7 d. This treatment also served as a precaution against enhanced Ar diffusion and/or solubility due to possible near-surface damage to the quartz lattice introduced during polishing (although the polish imparted by colloidal silica results more from chemical etching than physical abrasion). FTIR spectra of the polished quartz slabs taken before and after the preannealing treatment indicated virtual elimination of hydrous species, with the exception of hydroxyl associated with Al in the natural quartz crystals (Aines and Rossman, 1984, 1985). Ultimately, we learned that neither of these potential complicating factors—hydrous species dissolved in the quartz or possible near-surface lattice damage—has any impact on the measurements. This was demonstrated by running several experiments on specimens with natural, unadulterated growth surfaces (facets) and others on specimens that were ground and polished but not preannealed. Neither of these alternative approaches yielded results in any way distinguishable from the bulk of the data.

2.2.2. Experimental procedures

Most experiments were run in Stellite cold-seal pressure vessels of 9.5-mm inside diameter. To initiate an experiment, one or more polished quartz slabs were enclosed in a perforated Au envelope or tube and inserted into the pressure vessel, followed by a stainless steel rod to fill the remaining space. The vessel was connected to a pressure line, evacuated with a mechanical vacuum pump, and pressurized with Ar to a value close to the final desired run pressure of ~1 to ~185 MPa. The vessel was then placed in a horizontal tube furnace that had been preheated to the desired temperature (500–900 °C). The temperature rose to 85 to 90% of the final run temperature within ~20 min (depending somewhat on the target temperature); over this time interval, the pressure was bled off periodically to maintain a value close to the eventual run pressure. Once the system had stabilized, temperature was maintained to ±2 °C and pressure generally to within ~3% of the intended conditions. Pressure was monitored with a Heise Bourdon tube gauge in experiments above 20 MPa and with a pressure transducer with digital readout at lower pressures. In most cases pressure was controlled to significantly better than ±3%, but occasionally system leaks led to gradual pressure losses necessitating periodic upward adjustments. One experiment (no. 17; see Table 1) experienced significant Ar leakage, leading to pressure excursions of ~ 8% from the time-integrated average of 185 MPa. Viewed in the context of the inherent uncertainty in our diffusivity and solubility results, this pressure fluctuation in one experiment is of no significance. Quenching was achieved by removing the pressure vessel from the furnace and allowing it to cool in air. The resulting exponential temperature drop brought the sample below 200 °C in ~15 min; manual (upward) adjustments in pressure were made during this cooling interval to maintain P_{Ar} approximately constant.

Throughout the study, commercial-grade Ar was used as the pressure medium in preference to costlier high-purity gas for practical reasons—mainly because the pumping system is used for other gases and is not perfectly clean itself. Moreover, if minor impurities are important to the behavior of Ar with respect to quartz, then little understanding of natural systems is obtained from the study of an ultrapure system. As a precaution, we ran a qualitative mass-spectrometric analysis of the Ar we used and found CO_2 as the main impurity at a level well below 1%. Given that some piston-cylinder experiments involved C-O-H fluid is the Ar source (see below), the minor impurities in the Ar gas used in the cold-seal runs are considered insignificant.

Seventy-two individual quartz samples were run in cold-seal pressure vessels as described above. The data from these samples constitute the mainstay of this study, but several additional runs were made in a piston-cylinder apparatus to explore higher total pressures (1 GPa) and other sources of Ar. We used a 19-mm-diameter pressure assembly consisting of an NaCl outer sleeve, a Pyrex thermal insulator sleeve, and MgO filler pieces inside the graphite tube heater. The quartz samples were encapsulated in Pt sleeves lining holes in preoxidized Ni cylinders (see, e.g., Watson and Cherniak, 1997). At the start of an experiment, each quartz slab was packed in argonated hydroquinone or fullerene (see section 2.1). At run conditions, hydroquinone breaks down into reduced carbonaceous material plus a C-O-H-Ar fluid (H_2O was visible on opening most capsules). The argonated fullerene powder densifies at high T and P to amorphous carbon containing 3 to 5 wt.% Ar (no gas phase was apparent on opening the quenched capsules in this case). Argon uptake profiles were readily measured in quartz crystals in contact with these exotic Ar sources, although the quartz slabs were sometimes broken into two or three pieces on decompression and the surfaces etched by high P-T fluid (see section 3.1.3). Two piston-cylinder experiments were run at 500 °C and nine in the 800 to 900 °C range (one at 1.1 GPa, the rest at 1.0 GPa). A complete summary of both cold-seal and piston-cylinder experiments is included in Table 1.

2.2.3. Validation experiments

Several experiments were run to satisfy what we regard as necessary criteria for a high-quality diffusion study, the most important being a time series in which it is demonstrated that the measured diffusivity is independent of experiment duration over a large range in duration. To this end, four experiments (nos. 9, 32, 33, and 34 involving 13 total quartz samples) were run at ~850 °C and 100 MPa for durations ranging from 65 to 452 h. To explore the additional possibility that the identity of the quartz (natural or synthetic) might affect the results, we included both natural and synthetic specimens among the samples used in the time series; of the 13 samples run, eight were cut from natural quartz crystals and five from the synthetic crystal.

In addition to the time series, we reversed the Ar diffusion process in four quartz samples to show that the diffusivity is independent of diffusion direction. "Out-diffusion" experiments were performed at atmospheric pressure on specimens that had been run previously in pressurized Ar (nos. 27a, 27b, 27g, 27j; see Tables 1, 2) and whose diffusive-uptake profiles had already been characterized. When reheated under conditions of low Ar partial pressure, a sample possessing an Ar diffusive-uptake profile as a result of "in diffusion" at high pressure should experience Ar loss at a rate governed by the same diffusivity. Two of the previously run samples (27g, 27j) were reheated

Table 1. Summary of run information and resulting Ar diffusivities and surface concentrations.

Run no.	T, °C	P, MPa	Time, h	Orientation[a]	logD	σ logD	Surf. conc., ppmw	σ Surf. conc.
2	607	110	166.7	//	−20.66	0.28	2470	590
8a	811	140	121.5	//	−20.29	0.35	1690	590
8b	811	140	121.5	⊥	−20.19	0.10	4000	590
9a	852	100	65.0	//	−20.34	0.29	1970	530
9b	852	100	65.0	⊥	−20.33	0.22	2750	650
11a	790	100	95.5	//	−20.76	0.11	8870	850
11b	790	100	95.5	⊥	−20.50	0.17	3150	630
12a	882	100	44.0	//	−20.32	0.30	2430	570
12b	882	100	44.0	⊥	−19.85	0.27	1970	530
13a	685	100	191.7	//	−20.84	0.27	3410	770
13b	685	100	191.7	⊥	−21.05	0.29	2350	670
14a	647	100	168.0	//	−20.89	0.30	1810	510
14b	647	100	168.0	⊥	−20.93	0.17	3430	630
15a	760	100	165.0	//	−21.07	0.11	19800	1200
15b	760	100	165.0	⊥	−20.30	0.12	4640	790
17a	758	185	93.0	//	−20.59	0.19	3740	630
17b	758	185	93.0	⊥	−20.51	0.19	2050	390
20a	761	50	145.0	//	−20.59	0.07	9110	790
20b	761	50	145.0	⊥	−20.61	0.11	4860	670
22a	850	55	67.0	//	−20.55	0.13	5960	790
22b	850	55	67.0	⊥	−20.04	0.20	2190	550
24a	500	100	288.0	//	−21.11	0.21	3150	570
24b	500	100	288.0	⊥	−21.70	0.41	3130	670
27a	752	103	160.0	nat pyr[b]	−20.61	0.13	6080	850
27b	752	103	160.0	nat //[c]	−20.78	0.13	6280	930
27c	752	103	160.0	nat //[c]	−20.65	0.23	3230	770
27d	752	103	160.0	//	−21.20	0.10	37500	1800
27e	752	103	160.0	⊥	−21.00	0.30	2010	570
27f	752	103	160.0	//	−21.04	0.34	3170	830
27g	752	103	160.0	⊥	−20.86	0.32	2210	510
27h	752	103	160.0	//	−20.92	0.31	1950	510
27i	752	103	160.0	⊥	−20.77	0.42	1990	510
27j	752	103	160.0	//	−20.97	0.26	2870	710
27k	752	103	160.0	⊥	−21.02	0.36	2770	710
28a	891	100	20.5	//	−20.24	0.25	3330	530
28b	891	100	20.5	⊥	−20.07	0.36	2430	670
29a	893	100	118.0	//	−20.61	0.26	2270	530
29b	893	100	118.0	⊥	−20.56	0.22	1590	330
32a	850	100	67.0	⊥	−20.27	0.38	1910	570
32b	850	100	67.0	//	−20.57	0.40	1630	590
32c	850	100	67.0	⊥	−20.65	0.38	2470	730
33a	850	100	185.0	//	−21.15	0.36	1850	430
33b	850	100	185.0	⊥	−20.82	0.34	1950	510
33c	850	100	185.0	//	−21.05	0.47	1550	510
33d	850	100	185.0	⊥	−20.40	0.41	1590	510
34a	850	100	452.0	//	−20.92	0.50	990	430
34b	850	100	452.0	⊥	−20.87	0.46	1510	530
34c	850	100	452.0	//	−20.65	0.30	2410	890
34d	850	100	452.0	⊥	−21.15	0.52	1890	710
35a	550	103	281.0	//	−21.53	0.29	1850	430
35b	550	103	281.0	//	−21.55	0.27	2470	470
35c	550	103	281.0	⊥	−21.46	0.62	1010	430
36a	750	11.8	53.0	//	−20.52	0.20	4980	730
36b	750	11.8	53.0	⊥	−20.16	0.39	2430	630
36c	750	11.8	53.0	//	−20.26	0.30	2110	630
36d	750	11.8	53.0	⊥	−20.39	0.51	670	370
37a	748	20	44.5	//	−20.76	0.30	1810	410
37b	748	20	44.5	⊥	−20.34	0.75	710	370
37c	748	20	44.5	//	−20.55	0.31	2070	490
37d	748	20	44.5	⊥	−20.40	0.26	2130	450
38a	747	2.8	93.5	//	−20.73	0.20	2950	550
38b	747	2.8	93.5	//	−21.29	0.34	2610	510
38c	747	2.8	93.5	⊥	−20.64	0.32	1650	430
38d	747	2.8	93.5	⊥	−20.91	0.30	2570	550
39a	750	1	48.0	//	−20.04	0.75	1410	530
39b	750	1	48.0	⊥	−20.13	0.36	1370	470

(*continued*)

Table 1. (*continued*)

Run no.	T, °C	P, MPa	Time, h	Orientation[a]	logD	σ logD	Surf. conc., ppmw	σ Surf. conc.
39c	750	1	48.0	//	−20.20	0.32	2050	530
39d	750	1	48.0	⊥	−20.42	0.31	1590	410
45[d]	750	0.1	25.0	⊥	−20.65	0.45	zero	-
46[d]	750	0.1	25.0	//	−21.00	0.40	zero	-
47[d]	1200	0.1	3.5	pyramid	−19.59	0.32	zero	-
48[d]	1100	0.1	5.0	//	−19.98	0.38	zero	-
49a[e]	25	113	1.0	⊥	-	-	-	-
49b[e]	25	113	1.0	//	-	-	-	-
50a[e]	652	156	0.5	⊥	-	-	-	-
50b[e]	652	156	0.5	//	-	-	-	-
				piston-cylinder experiments				
1a[cl]	900	1000	43.5	⊥	−19.34	0.14	4310	890
1b[fu]	900	1000	43.5	⊥	−19.82	0.31	1080	360
4c[cl]	900	1100	6.0	//	−19.09	0.14	6290	740
5a[fu]	900	1000	12.0	//	−19.57	0.15	3400	500
5c[cl]	900	1000	12.0	//	−19.79	0.28	1970	440
5d[cl]	900	1000	12.0	⊥	−19.90	0.53	850	340
6b[cl]	800	1000	17.5	|	−19.46	0.18	2010	530
16[cl]	850	1000	22.5	⊥	−19.58	0.21	2180	520
18[cl]	850	1000	48.0	//	−20.29	0.24	1800	390
23a[cl]	500	1000	307.0	//	−21.48	0.25	730	160
23b[cl]	500	1000	307.0	⊥	−21.11	0.30	850	240

[a] Orientation of quartz slab relative to the c crystallographic axis.
[b] Natural pyramid face.
[c] Natural prism face.
[d] Out-diffusion experiment.
[e] Zero-time experiment.
cl Clathrate source (see text).
fu Fullerene source (see text).

at 750 °C and 1 atm for 25 h, one buffered at nickel–nickel oxide (run 45), the other in air (run 46). Two others (27a, 27b) were reheated in air at 1200 and 1100 °C for 3.5 and 5.0 h, respectively (these are run nos. 47 and 48; see Table 1).

An additional type of validation experiment included one that addressed the possible role of surface preparation and preannealing history on the outcome of the diffusion/solubility experiments. In a single cold-seal run at ~750 °C and ~100 MPa (no. 27), we included 11 separate quartz samples prepared in various ways from four different natural crystals and one synthetic crystal. The characteristics of these samples are detailed in Table 2.

The final confirmational experiments were two zero-time runs (nos. 49, 50) in which specimens of synthetic quartz oriented ⊥ and //c were prepared in the usual way (cut, polished, and annealed) and subjected to 113- to 156-MPa Ar. In run 49, the samples were held at pressure for 62 min but never heated, and in run 50 they were heated over the course of 18 min from room temperature to 652 °C, then cooled to room temperature in ~10 min by directing a jet of water against the pressure vessel.

2.3. Argon Depth Profiling and Data Extraction

2.3.1. Rutherford backscattering spectroscopy (RBS)

Numerous other diffusion studies in our lab reported over the past 10 yr have taken advantage of the unique depth-profiling capabilities of RBS. The main asset of the technique is its excellent spatial resolution in the direction of diffusion. Even with routine procedures and a standard surface-barrier detector, we achieve a depth resolution of ~10 nm. In practical terms, this means that a diffusant concentration at 40-nm depth is a discrete piece of information that is distinguishable from the concentration at 30- or 50-nm depth. The details of the

Table 2. Summary of information on quartz samples used in run 27.

Run ID	Crystal ID[a]	Slab orient.	Final polish[b]	Pre-anneal
27a	nat3	// pyramid	none (nat. facet)	none
27b	nat4	// prism	none (nat. facet)	none
27c	syn	// prism	none (nat. facet)	none
27d	nat2	⊥c	coll. SiO_2	none
27e	nat1	//c	coll. SiO_2	none
27f	syn	⊥c	coll. SiO_2	none
27g	syn	//c	coll. SiO_2	none
27h	nat2	⊥c	coll. SiO_2	1 wk, 1000°C
27i	nat1	//c	coll. SiO_2	1 wk, 1000°C
27j	syn	//c	coll. SiO_2	1 wk, 1000°C
27k	syn	⊥c	coll. SiO_2	1 wk, 1000°C

[a] "Nat1-nat4" represent quartz slabs cut from 4 different natural crystals; "syn" is a large synthetic crystal (see text).
[b] "Coll. SiO_2" = colloidal silica.

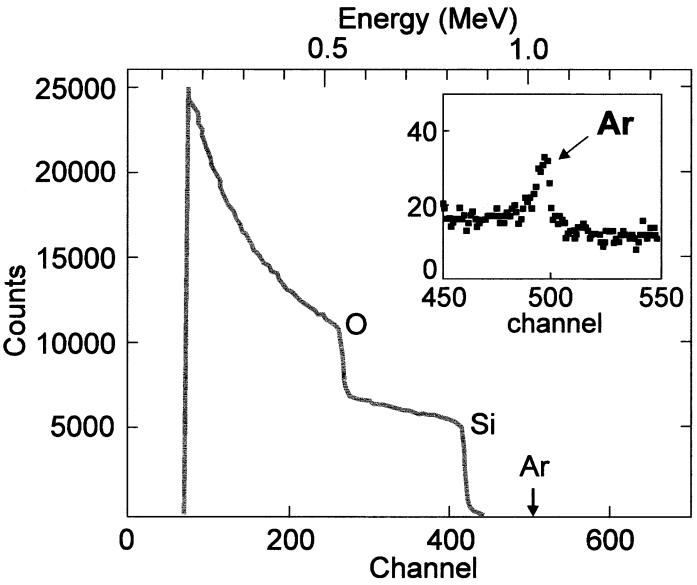

Fig. 1. A typical RBS raw spectrum from a quartz sample treated in pressurized Ar. Note the position of the Ar edge relative to those of Si and O. The region near the Ar edge is enlarged in the inset.

technique are described in previous papers (e.g., Chu et al., 1978; Cherniak and Watson, 1992; Cherniak, 1995). In brief, the method involves the use of a linear accelerator (in our case, at SUNY Albany) to direct 1 to 3 MeV $^4He^+$ ions at the surface of a sample into which the element of interest has diffused. The He^+ ions interact with the sample in several ways; in RBS the essential process is elastic backscattering, which occurs at the immediate surface and at depths up to a micron or more, depending on the elemental makeup of the target and the incident He^+ energy. The key to acquiring compositional information as a function of depth is that the energy of a detected (backscattered) He^+ ion depends on the mass of the nucleus it collided with and the depth in the sample at which that collision occurred (the latter because the He^+ ions lose energy through inelastic processes as they travel back through the sample). Ideal circumstances for depth profiling by RBS are a heavy diffusant in a light (low-Z), pure matrix. Quartz is outstanding on the second point, and Ar is sufficiently more massive than Si and O to give a detection limit of ~200 ppmw. This analytical sensitivity falls far short of requirements for Ar analysis at natural abundance levels but is adequate in experimental studies where relatively high levels of Ar can be introduced into minerals.

Another potentially advantageous aspect of depth profiling by RBS is the averaging inherent in the analysis. The profiles obtained represent concentration as a function of depth averaged over a relatively large area—in our case ~1 mm^2 (smaller areas can be imaged when the yield is sufficiently high). The need for a large surface area can have negative consequences when sample size is limited; however, it is not a factor with our quartz specimens and turns out to be especially useful in our study because some regions of some samples contain submicron pores with which the diffusing Ar interacts. As we will show, the averaging aspect of the analysis makes it possible to obtain meaningful information even from these samples.

A final strong point of RBS is that it is essentially a standardless analytical technique: in the energy range where alpha scattering is Rutherford (as it is in this case for Ar), both the backscattered ion energy and the concentration of the target species can be quantified by analytical expressions derived from classic scattering theory. Energy calibration of the detector and multichannel analyzer is performed as a matter of routine during each analytical session. The few pitfalls of RBS aside, we tested our technique against the solubility data of Carroll and Stolper (1991) for Ar in SiO_2 glass. Specimens of preannealed GE214 SiO_2 glass were subjected to ~150-MPa Ar at 700 °C for 2 h and then cooled as rapidly as possible. Argon diffusion in SiO_2 glass is fast, and the quench rate of our apparatus was not sufficient to preserve the 700 °C equilibrium Ar concentration at the sample surface during cooling. Argon solubility increases significantly with decreasing temperature (see Carroll and Stolper, 1991), so diffusion into the near surface of the glass occurred during quench. The RBS profiles obtained from the samples closely resemble diffusive-uptake profiles generated in numerical simulations incorporating the temperature dependence of Ar solubility and diffusion reported by Carroll and Stolper (1991).

A typical RBS spectrum from one of the Ar diffusion run products is shown in Figure 1.

2.3.2. Extraction of diffusivities and solubilities

Diffusion of Ar into a quartz slab is assumed to conform to one-dimensional diffusion in an infinite half-space with constant surface concentration, governed by a concentration-independent diffusivity. Accordingly, diffusivities for the vast majority of experiments (i.e., those involving inward diffusion of Ar) were obtained by fitting the reduced RBS depth profiles to the appropriate equation (Crank, 1975):

$$1 - \frac{C_q}{C_{srf}} = \mathrm{erf}\left[\frac{X}{\sqrt{4D \cdot t}}\right] \quad (1)$$

where C_q is the concentration at some depth X into the sample, C_{srf} is the concentration at the surface (where $X = 0$), D is the diffusivity, and t is experiment duration. In this study, C_{srf} is taken as the solubility of Ar in quartz. It is important to note that C_{srf} is not an independently measured quantity; rather, it is recovered from fitting the entire diffusion profile extending many tens of nanometers into the quartz. For this reason, C_{srf} is unrelated to surface Ar observed in the zero-time experiments, whose depth-integrated total mass is very small (see Fig. 2a and section 3.1.2).

We used the conventional approach of plotting the inverse error function of the term containing the concentration ratio—i.e., $\mathrm{erf}^{-1}[1 - C_q/C_{srf}]$—against depth, X. If the diffusion profile conforms to the assumed model, this plot should yield a straight line with slope $(4D \cdot t)^{-1/2}$. Linear regression is then used to obtain the slope and calculate D. The one semiadjustable parameter in this fitting approach is C_{srf}, which is not exactly known going into the inversion. However, a good guess at the surface concentration can be made by inspection of the diffusion profile. If the intercept of the regression of $\mathrm{erf}^{-1}[1 - C_q/C_{srf}]$ vs. X deviates significantly from zero, we simply iterate (using an adjusted C_{srf}) until a zero intercept is obtained. Because there is uncertainty in both concentration and distance, we use a regression algorithm that accommodates errors in both variables, similar to that of York (1969). The uncertainties in the slope and intercept returned by

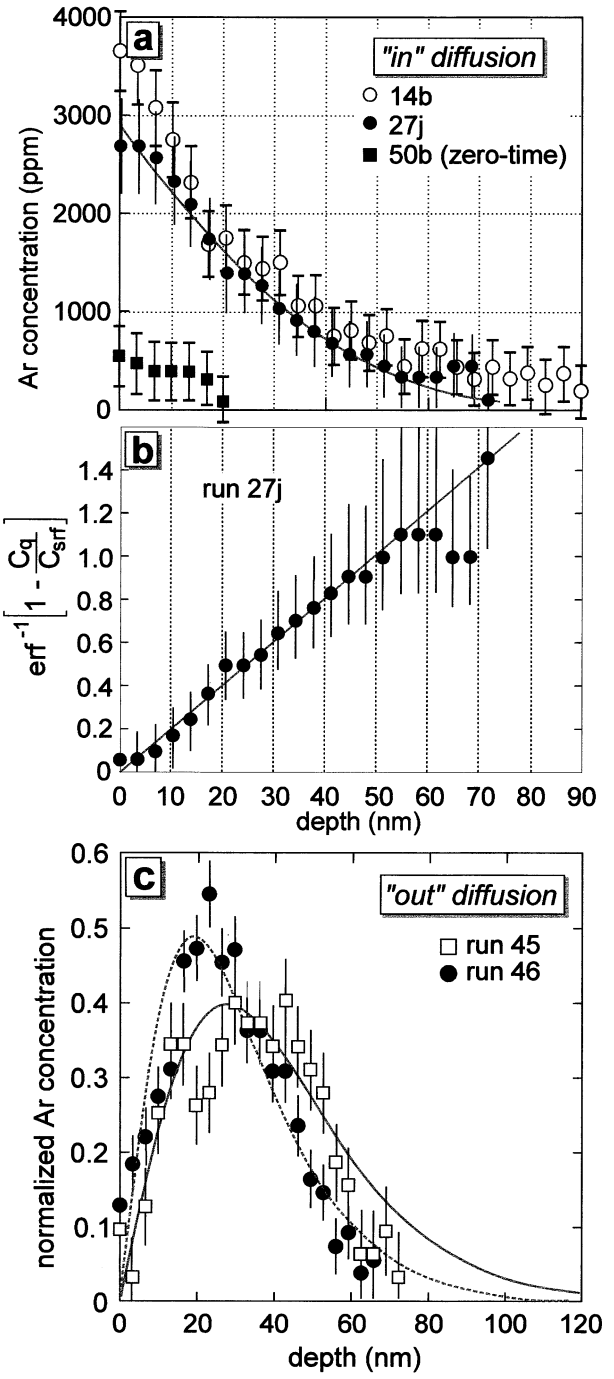

Fig. 2. (a) Typical uptake profiles resulting from in-diffusion of Ar into quartz in runs 14b, 27j, and 50a (error bars are $\pm 1\sigma$). Run 50b is a zero-time experiment at P-T conditions comparable with those of run 14b. The actual length of the 14b profile is highly uncertain (at 2 to ~10 nm) because of limitations in detector resolution; however, the integrated area under the curve is clearly small (see text for discussion). The smooth curve is the fit to the 27j profile. (b) Linearized version of the 27j profile obtained by inverting the concentration vs. depth data through the error function as explained in the text. (c) Ar out-diffusion profiles obtained by reheating quartz slabs from runs 27g (new run 45) and 27j (new run 46) at 750 °C and 1 atm for 25 h. Note the diffusive loss of Ar from the outer 20 to 30 nm. See text for discussion.

the linear fit can be converted into uncertainties in D and C_{srf}, respectively. The uncertainties are relatively large in this study, mainly because the backscatter yields are low and the counting statistics are unfavorable (i.e., the Ar concentrations are not far above the detection limit). The uncertainty ($\pm 2\sigma$) in $\log_{10}$D obtained from a single diffusion profile is typically ± 0.4 to 0.8 log units; that in C_{srf} is ± 40 to 60% (see Table 1). The overall robustness of our diffusion dataset thus depends more on the large number of experiments performed than on the accuracy of any one number. A good feeling for the interexperiment reproducibility of D can be obtained from run number 27. As noted earlier, this run included 11 samples run at exactly the same conditions, with a resulting mean $\log D_{Ar}$ of -20.89 ± 0.36 (2σ; D in m^2/s). The reproducibility of C_{srf}, representing Ar solubility, is more difficult to evaluate, because there is strong circumstantial evidence that Ar uptake is occasionally affected by small-scale porosity in the quartz. As discussed below, this porosity has a large effect on C_{srf} but little effect on D. Typical in-diffusion profiles and the linearized equivalent for one of them are shown in Figure 2 with appropriate error bars indicating the uncertainty in C_q, due to counting statistics, at all points along the profile.

Because the out-diffusion profiles are short (20–30 nm; see Fig. 2c) and the concentrations at each depth have inherently large uncertainties, no attempt was made to fit them to an analytical expression. In these cases we estimated the diffusivity based on the integrated amount of Ar diffused out of the sample.

3. RESULTS

3.1. Diffusion

3.1.1. Overall systematics

The diffusivities calculated from 83 Ar depth profiles are summarized in Table 1 and plotted on Arrhenius diagrams in Figure 3. Figure 3a summarizes 72 relatively low-pressure (1–185 MPa) data from the cold-seal experiments only and includes a linear fit with an envelope of uncertainty:

$$D = 8.2^{+8.8}_{-4.2} \times 10^{-19} \exp[(-6150 \pm 750)/T(K)] \qquad (2)$$

where D is in m^2/s. Despite significant scatter of the individual D values, there are enough data to constrain the activation energy reasonably well: it is low (51 kJ/mol) with an acceptable though not enviable uncertainty of $\pm 12\%$ at the 2σ level. Diffusivities perpendicular and parallel to the *c* crystallographic axis are indistinguishable, and no effect of the transition from α to β quartz can be discerned. For reasons discussed below, the high-pressure data are plotted separately (Fig. 3b) in comparison with the low-pressure Arrhenius line.

Figure 4a shows the diffusion results for the 11 samples run as experiment number 27 (752 °C, $P_{Ar} = 103$ MPa; see Tables 1 and 2). Despite differences in the sources of the quartz slabs and in their surface preparation and preannealing histories (hence, in "water" content), the resulting Ar diffusivities are the same within uncertainty. The three specimens whose surfaces are natural growth forms (nos. 27a, 27b, 27c) have a mean diffusivity that is slightly higher than the overall mean, but this is probably due to surface roughness on the natural growth forms that is not present on the polished specimens (RBS analysis of a rough surface would give a slightly elevated apparent diffusivity because of local variations in the He^+ beam incidence and backscattering angles). The diffusivity obtained from sample 27d, although within uncertainty of the other 10 samples, stands out slightly as the lowest value. As discussed below, this marginally lower apparent value probably results from nanopores in the quartz.

Diffusivities calculated from integrated Ar loss in the two out-diffusion experiments at 750 °C are indistinguishable from

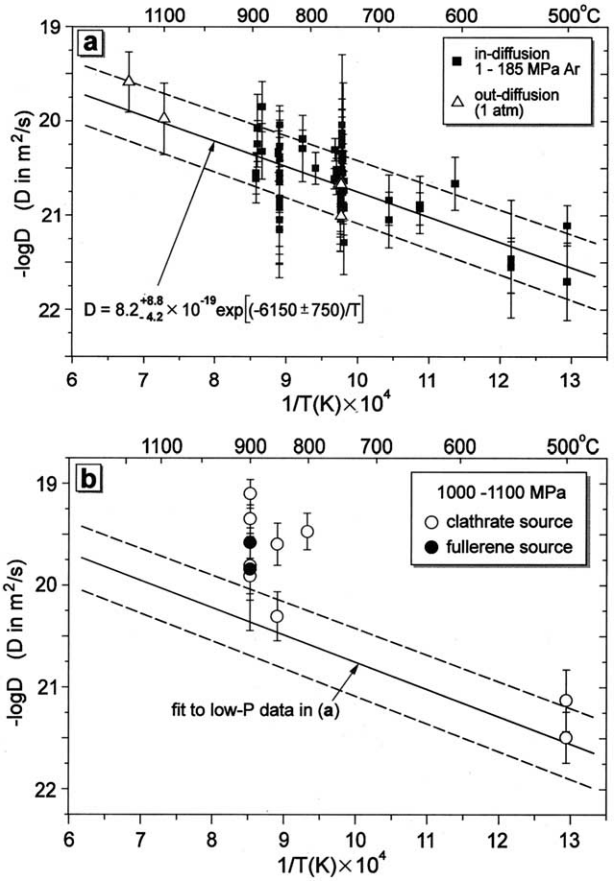

Fig. 3. (a) Arrhenius diagram summarizing diffusion data from 68 in-diffusion experiments run in cold-seal vessels at 1 to 185 MPa Ar plus four out-diffusion results at 1 atm (see text). In the equation for the least-squares fit, the constant in the exponential term (6150) corresponds to E_a/R—the activation energy divided by the gas constant. E_a thus has a value of 51 kJ/mol (12 kcal/mol). The confidence limits on the fit (dashed lines) are at the 2σ level. (b) Summary of diffusion data from piston-cylinder experiments in comparison with the data from (a). For reasons discussed in the text (section 3.1.3), the lower-pressure results are preferred.

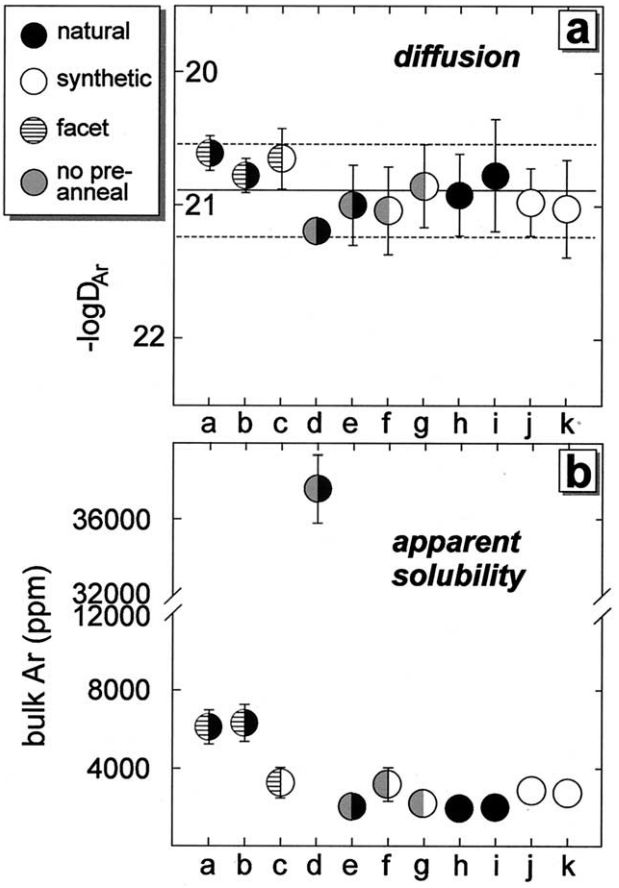

Fig. 4. Summary of Ar diffusivities (a) and apparent solubilities (b) from 11 different quartz slabs included in run 27 (752 °C, 103 MPa Ar pressure). The solid horizontal line in (a) represents the mean value of logD for the 11 samples (dashed lines above and below are $\pm 2\sigma$). See Table 2 for details concerning surface preparation and pretreatment of the 11 samples.

the bulk of the data (see Fig. 3). Model curves computed using the calculated diffusivities are superimposed on the actual depth profiles from these two runs in Figure 2c, from which it can be seen that the agreement is reasonable. The high-temperature, out-diffusion experiments (1100 and 1200 °C) also yielded results consistent with the bulk of the data. These two runs play an important role in the study in that they extend the temperature range by 300 °C above that where in-diffusion measurements could be made.

3.1.2. Time study and zero-time experiments

The results of the time series conducted at ~850 °C and 100 MPa Ar pressure are summarized in Figure 5. The experiments of relatively short duration (nos. 9, 32; 65 and 67 h, respectively) yield a slightly higher mean diffusivity, but one that is nevertheless within the uncertainties of the values resulting from the longer experiments. Because of limitations in detector resolution, the RBS peak representing diffusive uptake of Ar is slightly broadened; this effect causes minor increases in the apparent diffusivities when the profiles are short. No statistically significant time dependence of the Ar diffusivities is indicated; indeed, the mean values for the 185- and 452-h experiments are almost identical ($\log D_{Ar} = -20.75$ and -20.86, respectively).

Insufficient depth resolution also prevented accurate profiling of the zero-time experiments. In both runs (49, 50) an Ar signal of a few channels width, statistically just above background, was apparent in the RBS spectra (see Fig. 2a), indicating the presence of appreciable Ar in the very near-surface region of the samples. However, Ar penetration into the quartz lattice was extremely limited. Based on the energy resolution of the α detector, it can be concluded that Ar resides in a surface layer not exceeding 10 nm in thickness in the zero-time run products (the apparent penetration to ~18 nm in Fig. 2a is a result of analytical spreading due to limited detector resolution). Unfortunately, placing a lower bound on the thickness is not possible. If we assume that Ar penetrated the run-50 samples (which were heated briefly to 650 °C) according to our measured diffusivities (Eqn. 2), the total length of the expected diffusive uptake profiles is ~2 nm. In the case of run 50, then,

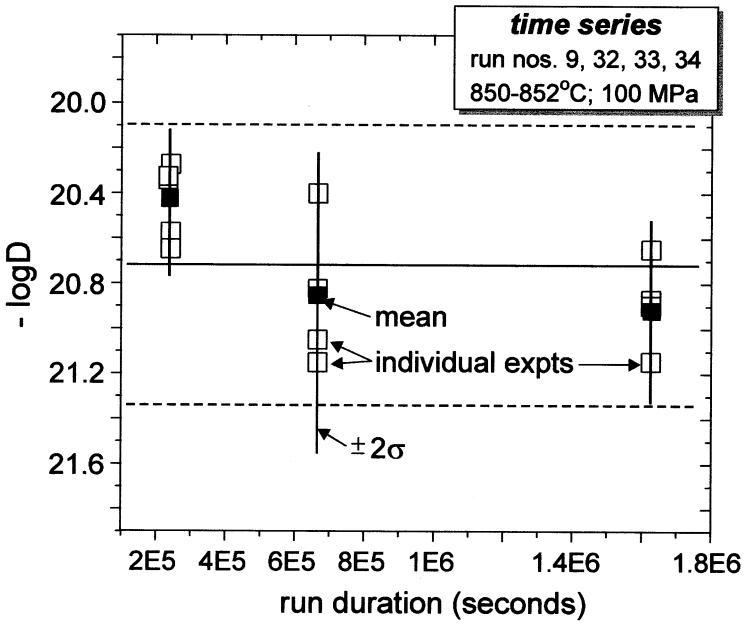

Fig. 5. Argon diffusivities obtained in a times series at ~850 °C and 100 MPa Ar pressure. The solid horizontal line is the mean of the 13 individual D values; dashed lines are $\pm 2\sigma$.

the profile length is effectively bracketed between ~2 and 10 nm. Without better knowledge of penetration depth, the concentration of Ar at the surface cannot be determined; however, the total amount of Ar can be estimated—with large uncertainty—by the integral under the zero-time curve in Figure 2a.

The run-49 samples (pressurized in Ar but not heated) yield spectra that are indistinguishable in terms of penetration depth from run 50, but somewhat higher Ar concentrations are suggested. In this case, penetration of Ar into the normal quartz lattice by diffusion is precluded because the room-temperature diffusivity is too low (the characteristic diffusion distance, $x \sim (D \cdot t)^{1/2}$, is a fraction of an Angstrom unit). This leaves a limited number of possible interpretations: the argon is either (1) adsorbed on the surface, (2) diffused into a near-surface, structurally anomalous layer < 10-nm thick, or (3) both of the above. If the argon is simply adsorbed, it is bound to the quartz surface sufficiently well to preclude loss over a period of days at atmospheric conditions followed by hours in the high vacuum of the accelerator beam line. We favor the interpretation that Ar in the cold, zero-time samples resides at least partially in a thin, near-surface layer that differs somewhat in structure from the bulk quartz lattice. X-ray reflectivity studies establish the thickness of this layer as 1.4 nm (Schlegel et al., 2002; see discussion in section 4.2.2).

The overall results of the zero-time experiments are consistent with the bulk of the experiments described in this paper, given the limitations in depth resolution of the RBS method. The most important conclusion to be drawn from them is that the integrated amount of Ar in the structurally anomalous surface layer is very small relative to the amount that diffuses into the quartz lattice during an experiment of extended duration (see Fig. 2a). Argon in this layer thus has a negligible effect on solubility in the quartz lattice as deduced mathematically from the extended diffusion profiles.

3.1.3. High-P results and implications

Argon diffusivities obtained from the 11 piston-cylinder runs at P_{total} = 1.0 or 1.1 GPa plot close to the low-pressure Arrhenius line (Fig. 3b), but there are systematic differences between the two datasets. The two high-pressure values at 500 °C fall on the low-pressure line within uncertainty, but most of the data at 800 to 900 °C lie above the line by up to 1 log unit. This difference is noted in the interest of full disclosure, but we consider the cold-seal dataset to be more reliable because of inevitable degradation of the quartz specimens recovered from piston-cylinder runs. These are often fractured on decompression, and the surfaces of those exposed to C-O-H fluid (clathrate Ar source) at run conditions are roughened by dissolution etching, especially at the higher temperatures. Both of these problems degrade the quality of the RBS spectra: the analyzed area is reduced by having to work with sample fragments, and the surface roughening broadens the element edges in the spectra. The latter effect is especially significant, because it can lead to high apparent diffusivities. Because the quartz samples recovered from cold-seal runs do not suffer from these problems, and because the piston-cylinder results are not in fact very different from the bulk of the data, we advocate use of the low-pressure Arrhenius line for geochemical applications.

Sample problems and small differences in the data aside, the broad agreement between the low- and high-pressure data leads to two important conclusions: (1) there is not a major effect of total pressure on Ar diffusion in quartz over the range of conditions encountered in the Earth's crust and (2) any influence of H-bearing species or P_{H2O} is also small (this latter finding is true of K-feldspar as well; see Foland, 1974; Wartho et al., 1999). The latter conclusion is reached at this juncture based on the similarity between piston-cylinder results obtained with the C-O-H fluid (clathrate) Ar source and the results of

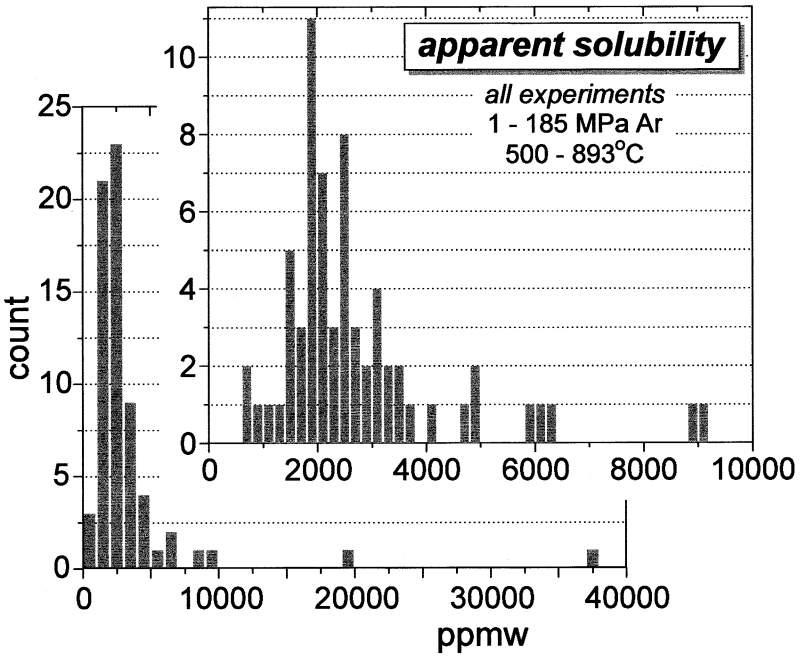

Fig. 6. Histograms summarizing apparent solubilities of Ar in quartz estimated from the surface concentrations in the diffusive-uptake profiles. The anomalously high values are attributed to the occasional presence of Ar-filled nanopores in the near-surface region (see text and Figs. 7 and 8).

numerous, nominally dry, cold-seal experiments. However, the absence of a P_{H_2O} effect is also apparent from the fact that the clathrate (wet) and fullerene (nominally dry) Ar sources yield indistinguishable results at the same pressures (see Fig. 3b).

In conclusion, it seems clear that no major variations of Ar lattice diffusion systematics in quartz occur over the range of pressure and C-O-H fluid composition encountered in the Earth's crust.

3.2. Solubility of Ar in Quartz and the Role of Nanopores

As noted previously, the near-surface concentration of Ar in a quartz sample equilibrating with pure Ar gas should, in principle, represent the solubility of Ar in the quartz lattice. We had hoped to use the surface concentrations extracted from our RBS spectra as estimates of Ar solubility that are quantitative within the uncertainty of the analyses and data reduction (see section 2.3.2). This approach was successful in the end, but the data interpretation was complicated by the occasional observation of very high apparent solubilities. The problem is dramatically illustrated by Figure 4b, which shows apparent solubilities of Ar in quartz for the 11 samples run simultaneously as experiment number 27 (since these were run in the same pressure vessel at the same time, there is no question that the P-T conditions and gas medium were identical in every respect). Ten of the 11 samples show apparent solubilities in the ~2000- to 6000-ppm range, and eight of these fall in the ~2000- to 3000-ppm range (these eight are actually the same within analytical uncertainty; see section 2.3.2 and Table 1). The two samples with apparent solubilities of ~6000 ppm (27a, 27b) are outliers and would require explanation even if they were not totally overshadowed by sample 27d, which has a surface concentration approaching 4 wt.% Ar. This is by far the highest value we encountered in the entire study, but there are a few others exceeding 8000 ppm as shown in the histograms of Figure 6. Because it represents an equilibrium quantity, the true solubility of Ar in the quartz lattice must be reproducible at a given P and T. The surface concentrations measured in this study, although generally reproducible within the substantial analytical uncertainty, show occasional positive excursions that point to a sporadic complicating factor in the uptake of Ar in quartz. Note that among the 11 samples in run 27, the three exhibiting anomalously high apparent Ar solubilities do not correlate with crystal identity, surface preparation, or preannealing history. Also noteworthy is the fact that all 11 samples give essentially the same diffusivity, although 27d, with its very high surface concentration, has the lowest diffusivity (see Fig. 4).

Only 12 of the 66 apparent solubilities obtained from the cold-seal experiments are truly anomalous in that they lie above the estimated $+2\sigma$ uncertainty (that is, above ~3500-ppm Ar). It is tempting simply to disregard the high values as spurious and reduce the dataset accordingly. We took the opposite approach of trying to determine the cause of the sporadic anomalies, believing that the explanation may be important to understanding Ar behavior not only in the laboratory but also in nature. The observations in the previous paragraph led us to a simple explanatory model, which we tested in several ways. In brief, our interpretation is that the quartz crystals used in the study (both natural and synthetic) have occasional, localized regions that are porous on a very small scale. Since the crystals used in the study are all of hydrothermal origin, the word "pore" is probably synonymous with the term "fluid inclusion" for most purposes. Quartz slabs with visible fluid inclusions were screened out at the start of our study, but it now seems

probable that the inclusions range down to extremely small size and sparse density, making them undetectable by ordinary means. When a porous region fortuitously intersects the surface of a sample used in an Ar-uptake experiment, the effect on the apparent Ar solubility can be dramatic.

Very small fluid inclusions ($\ll 1\mu$m) probably would not decrepitate during the preannealing treatment at 1000 °C and 1 atm pressure (see discussion in Roedder, 1984); rather, they would lose water by molecular diffusion through the quartz lattice (Zhang et al., 1991). By this process, small aqueous fluid inclusions in the preannealed samples would become true pores, essentially devoid of fluid at the start of the Ar in-diffusion experiments.

The literature contains circumstantial evidence for the presence of very small fluid inclusions in quartz. FTIR spectroscopy has revealed freezable water in samples lacking visible fluid inclusions (Aines and Rossman, 1984). That this water is freezable indicates that it is a free fluid—i.e., it does not consist of individual water molecules dissolved interstitially in the quartz lattice. Pores of submicron size have been directly imaged in other minerals, most notably feldspars (see, e.g., David and Walker, 1990; Montgomery and Brace, 1975). Turbidity attributed to the presence of submicron pores or "channels" in feldspars has been correlated with laboratory Ar loss characteristics (e.g., Parsons et al., 1988).

Some of the characteristics of the hypothetical pores in our quartz samples were deduced indirectly. Most important to Ar transport is the fact that they must be isolated from one another, since interconnected pores would lead to vastly more rapid Ar uptake. The quartz samples having the highest Ar surface concentrations (by inference, the most porous ones) actually may have marginally lower bulk diffusivities than the rest of the samples, if they differ at all (see Fig. 4). We were unsuccessful in attempts to image pores in our experimental run products using the secondary-electron imaging capabilities of our JEOL 733 electron microprobe, which places their size somewhere below ~0.1 to 0.2 μm. Even without an image, the average abundance of pores in the near-surface region of a given sample can be estimated based on two simple assumptions: (1) the near-surface concentrations from the RBS analyses are a composite of Ar in the quartz lattice plus Ar in closed pores and (2) the actual solubility of Ar in the quartz lattice is the minimum surface concentration observed in any sample at similar P-T conditions (say, ~2000 ppm at 750 °C and 100 MPa Ar; see Figs. 4 and 6). The Redlich-Kwong equation of state for Ar (Holloway, 1977) gives the molar volume of Ar in the near-surface pores, assuming these are equilibrated with the gas medium outside the quartz crystal. Given these assumptions, it can be shown that a porous quartz sample with a bulk Ar concentration of 1 wt.% must have a pore volume fraction of ~0.04. The weak point of this calculation is that the solubility of Ar in the quartz lattice is not known with certainty, and the assumed value of 2000 ppm might seem unreasonably high (if the solubility is only 200 ppm, then the calculated pore volume fraction is ~0.05). For reasons that will be substantiated in section 4.1, we believe that the actual lattice solubility is in fact quite high—if it were not, the diffusive flux through the quartz lattice would be too low to generate the observed high-Ar uptake profiles. High Ar solubility is not implausible given the open structure of the quartz lattice, and previous studies hint at high Ar solubilities in other minerals of similar structure: Laughlin and Yoder (1971), for example, diffused Ar into albite powder at 200 MPa Ar and raised the bulk concentration to ~200 ppm, even though the albite was far from fully equilibrated with the Ar pressure medium.

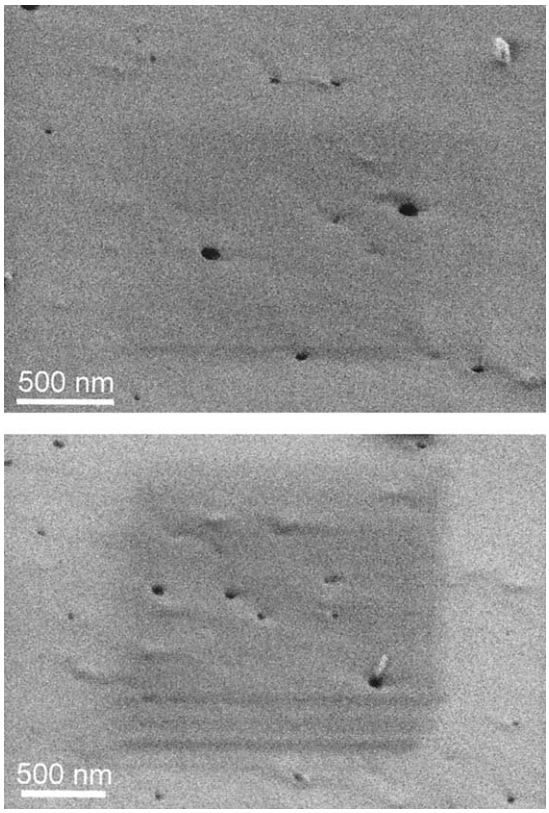

Fig. 7. Secondary-electron images of quartz fracture surfaces from run 15b taken with a JEOL 6435F scanning electron microscope. The darker rectangular patches centered in the images represent alteration to the surface by the electron beam during examination at higher magnification than was used for the photos.

Ultimately, the most convincing evidence that porosity plays a role in our apparent solubility measurements is presented in Figure 7, which comprises two field-emission SEM photomicrographs of fracture surfaces of a quartz specimen used in a diffusion experiment. The sample represented in the images (run no. 15b) exhibited an anomalously high apparent Ar solubility; it was crushed to create surfaces that had not been polished with colloidal SiO_2, which were then examined with a JEOL 6435 field-emission SEM in the Department of Materials Science and Engineering at RPI. There are numerous, nearly spherical pores in the images, ranging downward from ~70 nm in diameter. The smallest discernible pores are ~10 to 15 nm in diameter, and hence probably warrant the term "nanopore" (there may be others that are too small to resolve with our instrument). Visible pores are not ubiquitous, but they were detected at several locations on the fracture surfaces of this and one other sample. It should be noted that attempts to image pores on the surfaces of other samples that probably have them (judging from apparent Ar solubilities) were always unsuccessful, suggesting that the features are generally too small to see even with the field-emission SEM (i.e., they are significantly

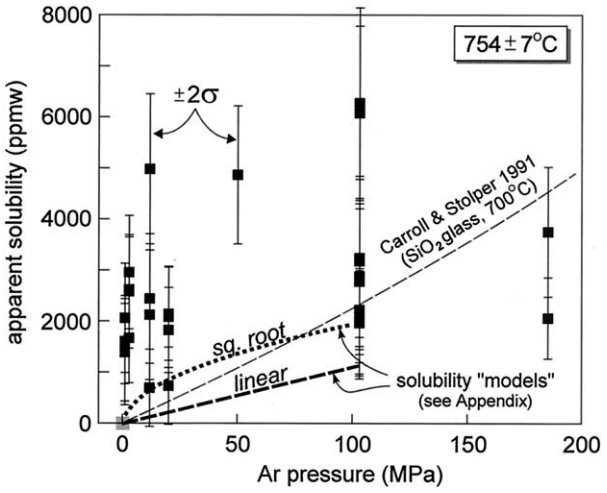

Fig. 8. Apparent solubilities of Ar in quartz plotted against Ar pressure. The crude solubility models used in the numerical simulations are shown as heavy dashed and dotted lines (see text and Appendix). The gray square at 0,0 is a constraint confirmed by the out-diffusion experiments—i.e., Ar concentration goes to zero at the surface when Ar-bearing quartz samples are heated at 1 atm. The light dashed line represents the solubility of Ar in silica glass as determined by Carroll and Stolper (1991). See also Figs. 4b, 6, and 9.

smaller than 10 nm). The size of the observable pores in Figure 7 should probably be regarded as an upper bound on the size of these features as they affect bulk Ar uptake in our quartz specimens. In the context of the length scales of the RBS analyses, the size of individual pores is insignificant relative to the area ($\sim$1 mm^2) sampled by the He beam.

Unfortunately, the presence of pores in a few samples, combined with the large inherent analytical uncertainty, makes it difficult to quantify Ar solubility in the quartz lattice at fixed pressure and temperature, let alone extract information on the P and T dependencies. However, some qualitative observations can be made from the existing data. Figure 8 shows apparent solubilities plotted against Ar pressure for 29 experiments at roughly the same temperature (747–761 °C). The dotted curve is a suggested lower boundary to the measurements that may approximate Ar solubility as a function of pressure (see Appendix). If this interpretation is correct, Ar appears to saturate the quartz lattice at a pressure somewhere below $\sim$100 MPa, because markedly higher pressure (185 MPa) still results in one value ($\sim$2000 ppm) equivalent to the lowest values at $\sim$100 MPa (an alternative, linear solubility relation is also shown on Fig. 8; see Appendix and section 4.1). Not unexpectedly, pressures in the 1 to 20 MPa range yield the lowest values, but the bulk concentrations are still well above the RBS detection limit. The one additional constraint on the pressure effect is that, as expected, the apparent solubility approaches zero at $P_{Ar} = 0.01$ MPa, as evidenced by the Ar profiles from the out-diffusion experiments (see Fig. 2c).

Included in Figure 8 is a curve representing the solubility of Ar in SiO_2 glass as determined by Carroll and Stolper (1991) (see their Fig. 11a). Perhaps surprisingly, our low-pressure data for quartz are consistent with the curve for glass at $P_{Ar} = 100$ MPa; in fact, the average of our lowest values falls essentially on the glass solubility curve. At higher pressures, the solubility of Ar in quartz falls well below that in SiO_2 glass, indicating a probable saturation of available sites, as noted above. The more precise data of Carroll and Stolper (1991) enabled them to treat their data in terms of a solubility model involving a fixed population of available sites or "holes." They concluded from this approach that the density of sites available for Ar occupancy in SiO_2 glass is at least 4×10^{20} sites/cm^3. Assuming Ar saturation is reached in quartz at $P_{Ar} = 100$ MPa (the saturation pressure could be significantly lower; see Fig. 8), similar reasoning applied to our data indicates an occupiable site density of $\sim 8 \times 10^{19}$ sites/cm^3. Given the difference in openness of the structures of SiO_2 glass and crystalline quartz, this difference in available site density seems reasonable.

No effect of temperature on the solubility of Ar can be discerned in our data, because it is masked by the large analytical uncertainty. It seems clear, however, that the solubility remains substantial down to 500 °C at 100 MPa, because there is still major diffusive uptake of Ar at these conditions.

4. DISCUSSION

4.1. Nanoporosity and Diffusion: Numerical Simulation

4.1.1. Overview and rationale

Figure 7 is a convincing indication that some of the quartz specimens used in our study are locally porous on a very small scale. However, this photograph is not representative, in terms of pores sizes, of the near-surface regions of the few samples showing high apparent Ar solubilities (because pores were not detected on the surfaces of these samples). The principal evidence for occasional pore involvement in the diffusive uptake of Ar thus remains circumstantial. We believe our diffusion results accurately reflect Ar transport in the quartz lattice (i.e., that the presence of pores in the profiled regions of some samples does not greatly impair our ability to obtain good diffusion data). We are also convinced that the solubility of Ar in the lattice is high and reasonably well approximated by our lowest apparent solubility measurements, simply because Ar could not fill isolated pores if it were not soluble in quartz. To strengthen our interpretations and conclusions, we undertook numerical simulations of diffusion in a medium that is sparsely populated by pores in which the diffusant is highly concentrated. This effort was considered worthwhile not only because it clarifies anomalous aspects experimental results, but also because it reveals characteristic behavior that may apply to noble gas behavior in natural crystals containing isolated pores. The approach is described in detail in the Appendix; here, we will simply review the results and implications of the modeling.

Our model system is a quartz crystal containing 1 to 5 vol.% pores, which is realistic in terms of the mass balance calculation described in section 3.2 (4% porosity is required for an apparent surface concentration of 1 wt.% Ar) and also by comparison with the SEM photographs in Figure 7. The quartz crystal is assumed to be at 700 °C and surrounded by Ar at 100-MPa pressure. According to our experimentally determined Arrhenius relationship, the diffusivity at this temperature is 1.6×10^{-21} m^2/s.

To our knowledge, no previous papers have addressed the systematics of bulk gas uptake into a mineral containing isolated pores, so we investigated several model scenarios to

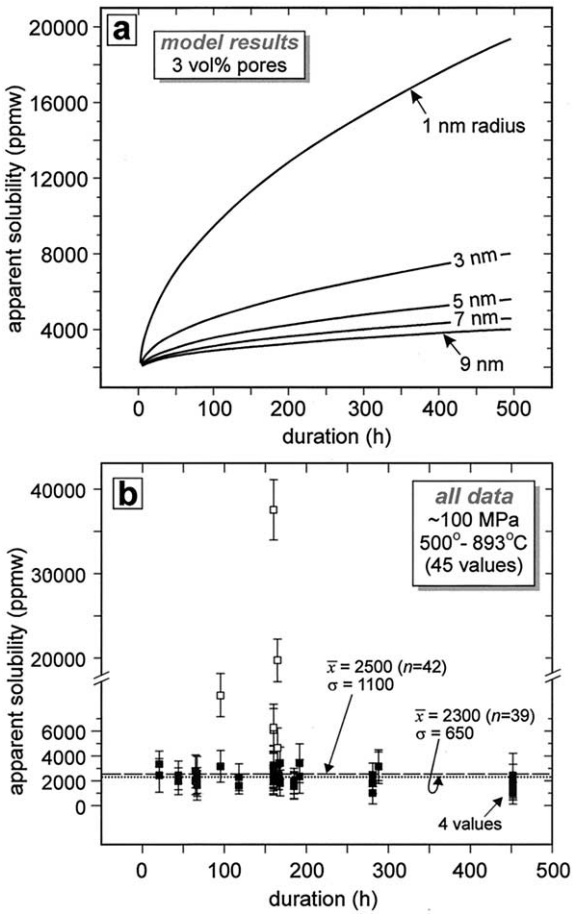

Fig. 9. (a) Results of numerical simulations of Ar diffusion into porous quartz showing variation with time of apparent Ar solubility (i.e., bulk concentration in lattice + pores) at the sample surface. In (b) the measured apparent solubilities at P_{Ar}~100 MPa are plotted against time. With only a few exceptions, the trend is a horizontal line within uncertainty, indicating a generally minor influence of pores on Ar uptake (see text).

ascertain what variables are important and to see how the bulk behavior might affect our experimental results.

4.1.2. Time dependence of apparent solubility

A distinguishing characteristic of gas diffusion into a porous medium is that the bulk concentration (gas + lattice) in the near surface must change with time as the pores just below the surface fill with gas (in samples lacking pores, the surface concentration is fixed by the lattice solubility). This difference provides a basis to test our overall results. Figure 9a shows model results for diffusion into quartz containing 3 vol.% pores ranging in size from 1 to 9 nm. The solubility of Ar in the quartz lattice is assumed to be 2000 ppm (this assumption is evaluated below; the immediate goal is to assess the variation in apparent solubility with time due to the influence of pores). Note in Figure 9a that pore size has a marked effect on the time variation of apparent solubility as represented by the bulk near-surface concentration. This is because, for a given porosity, small pores are closer together and have a higher total surface area than large ones. Pores of 9-nm radius cause a relatively subtle change in the apparent solubility; 1-nm pores have a dramatic effect. Figure 9b has the same axes as 9a, but the plotted values are the apparent solubilities obtained from all cold-seal runs at a constant nominal pressure of 100-MPa Ar (45 values in all). The emphatic message of this diagram is that, with the exception of three to six aberrant points (open symbols), there is no indication that the apparent solubility changes with experiment duration. Within the uncertainty of the measurements (and any effect of real variation due to differences in temperature), the overwhelming majority of the data define a horizontal line. This is taken as a strong indication that most of the apparent solubilities—although subject to considerable analytical uncertainty—are not rendered meaningless due to uptake of Ar in pores. The presence of isolated pores must lead to variation in apparent solubility with time, but this is not a characteristic of the overall dataset. Figure 9b further implies that the real solubility of Ar in quartz is not strongly temperature dependent.

4.1.3. Effect of pores on Ar uptake profiles

Because Ar uptake profiles in quartz form the basis of this study, we went on to use our modeling approach to assess the effect of pores on simulated bulk-diffusion profiles. For this purpose our model system was a quartz crystal containing up to 5 vol.% pores of various sizes. Figure 10 shows the results of a numerical diffusion experiment lasting 10^6 seconds (278 h), which is close to the median of our real experiments and about twice the mean duration. In Figure 10a, bulk diffusive uptake profiles are depicted for a lattice solubility of 2000 ppm, a worst-case porosity of 5%, and pore radii of 3, 5, and 10 nm. The "no-pore" case is shown for comparison. In Figure 10b, profiles are depicted that result from the presence of 1 to 2 vol.% pores ranging in size from 1 to 6 nm. The key conclusions to be drawn from Figure 10 are as follows: (1) much more Ar gets into the samples containing pores, (2) the overall penetration distance of Ar into quartz is not dramatically affected by the presence of pores, and (3) the apparent surface concentration in the quartz—which is actually the bulk concentration (quartz + pores) in the near-surface region of the sample—is sensitive to pore size (this is a pore surface area and spatial density effect).

The insensitivity of the overall diffusive length scale to the presence of pores is what makes it possible to extract meaningful lattice diffusion data even from a porous sample. This insensitivity results from the sparse density of pores and the fact that many diffusing Ar atoms do not encounter them on their way through the quartz lattice. Figure 11 illustrates the point. The numerically generated diffusion profile for pores of 10-nm radius is reproduced from Figure 10 and compared with the error function profile that would result from diffusion into a medium having the same high surface concentration and the same diffusivity (1.6×10^{-21} m^2/s) as the model system, but no immobilizing pores (see Fig. 11a). The profiles are noticeably different, but inversion of the model profile through the error function (as is done in reducing our "real" analytical data) nevertheless returns a diffusivity of 1.1×10^{-21} m^2/s, which differs by only ~30% from the lattice diffusivity governing the overall diffusion process (see Fig. 11b). The linearized version of the model profile representing bulk Ar in the composite medium (quartz + pores) is certainly not perfectly linear, but

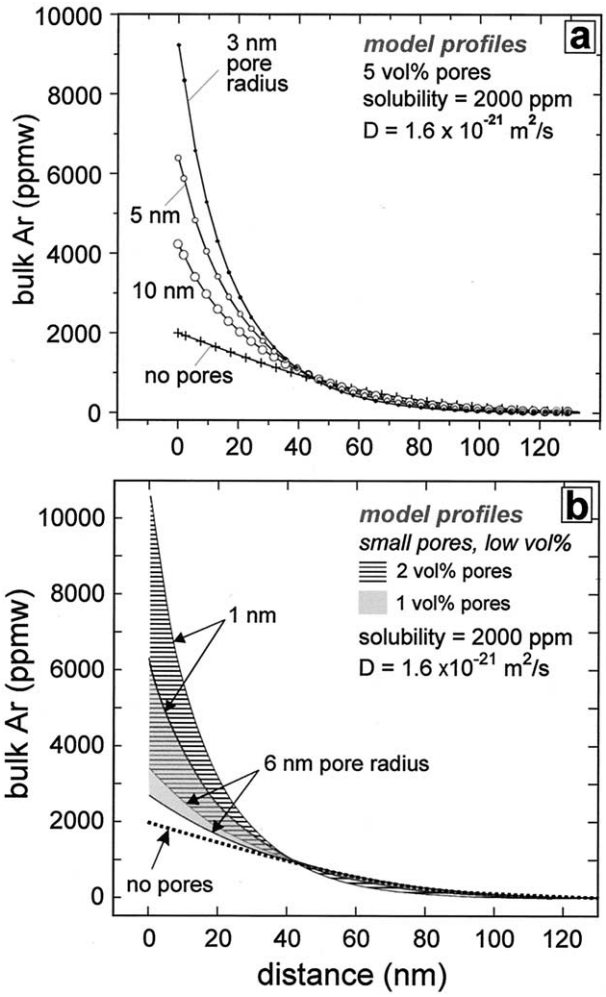

Fig. 10. (a)Numerically generated profiles resulting from Ar diffusion into quartz containing 5 vol.% pores ranging in size from 3- to 10-nm radius. The profiles represent bulk Ar concentration—i.e., Ar in the quartz lattice plus Ar in the nanopores. The other model parameters are shown on the figure. The quartz surface is at x = 0; the pore-free case is shown for reference. See text and Appendix for details. In (b) simulated profiles are shown for samples containing only 1 to 2% pores in the 1- to 6-nm size range.

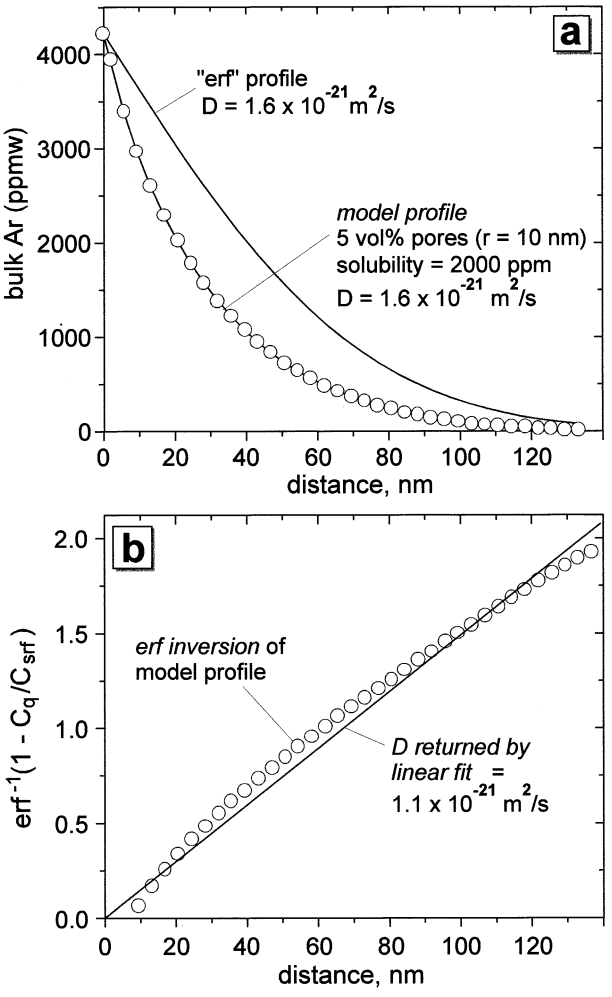

Fig. 11. (a) Bulk Ar-uptake profile resulting from diffusion into 5% porous quartz compared with the error-function profile that would result from diffusion into pore-free quartz having the same surface concentration. In (b) the model profile is inverted through the error function to show that the resulting Ar diffusivity differs by only ~30% from the actual lattice diffusivity.

the D extracted from it is close to that resulting from the error-function profile for pore-free quartz. The deviation from linearity, while obvious in Figure 11b, would not necessarily be detectable in practice (cf. Fig. 2). The small difference in D (~30%) is within the analytical uncertainty inherent in depth profiling Ar in quartz by RBS. Figure 11 establishes that meaningful diffusion data can be obtained from experiments in which the surface concentrations are not meaningful in the usual sense.

It is clear from the preceding discussion that the apparent solubility of Ar in quartz (as indicated by the bulk surface concentration, C_{srf}) is very sensitive to the presence of pores, but D is not. These conclusions were explored in more detail by running a series of simulations in which pore size and volume were varied systematically, and the consequences for both D and C_{srf} evaluated. As in the case of the simulations represented in Figure 10, the duration was set at 10^6 seconds, the lattice diffusivity at 1.6×10^{-21} m^2/s, and the lattice solubility at 2000-ppm Ar (see Figs. 8 and 9b re the choice of solubility). Note that because the apparent solubility (as given by the surface concentration, C_{srf}) can be highly time-dependent (Fig. 9a), the use of a relatively long duration maximizes the influence of any pores that might be present. The model results are shown in Figure 12. As anticipated, the effect of pores on the apparent solubility in a long experiment can be large (Fig. 12a), but even the worst-case effect on D (lots of tiny pores) is only about a factor of 4 (Fig. 12b).

4.1.4. Consequences of assumed low lattice solubility

For comparison with numerical results obtained assuming a high lattice solubility (2000 ppm; see Fig. 10), we ran additional simulations incorporating a relatively low solubility of 100 ppm. The results are shown in Figure 13. Briefly, if the solubility were indeed as low as 100 ppm, and the process governed by a diffusivity similar to our measured values, then very little Ar would get into the quartz—even with 3-nm pores;

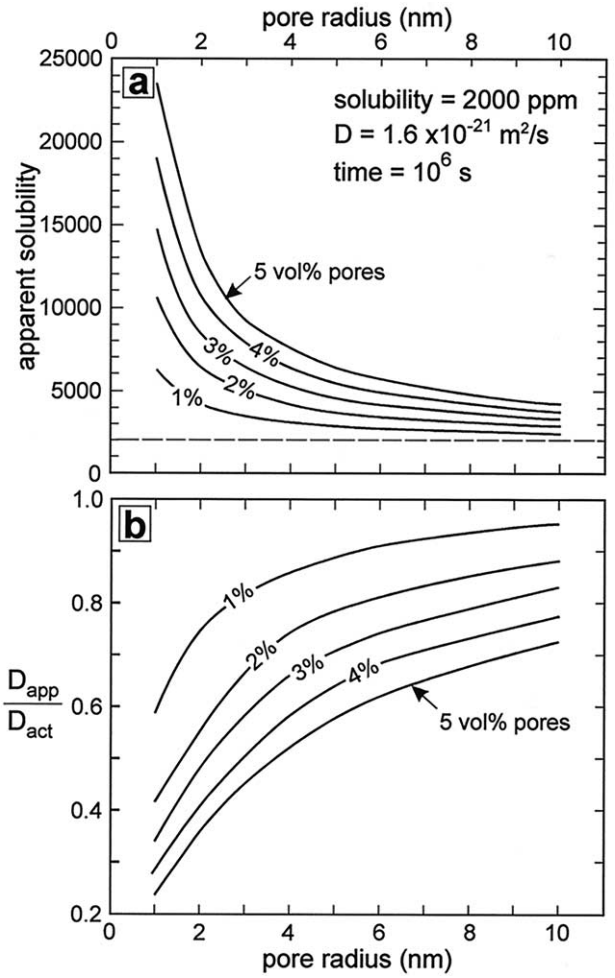

Fig. 12. Simulation results showing the effect of pores on the solubilities (a) and diffusivities (b) extracted from bulk-sample diffusive uptake profiles produced in experiments of 10^6 s duration. The actual solubility is assumed to be 2000 ppm, the lattice diffusivity 1.6 $\times 10^{-21}$ m^2/s. Note that the apparent solubility is dramatically affected by the presence of pores, but D is not. See text and Figs. 9 and 11.

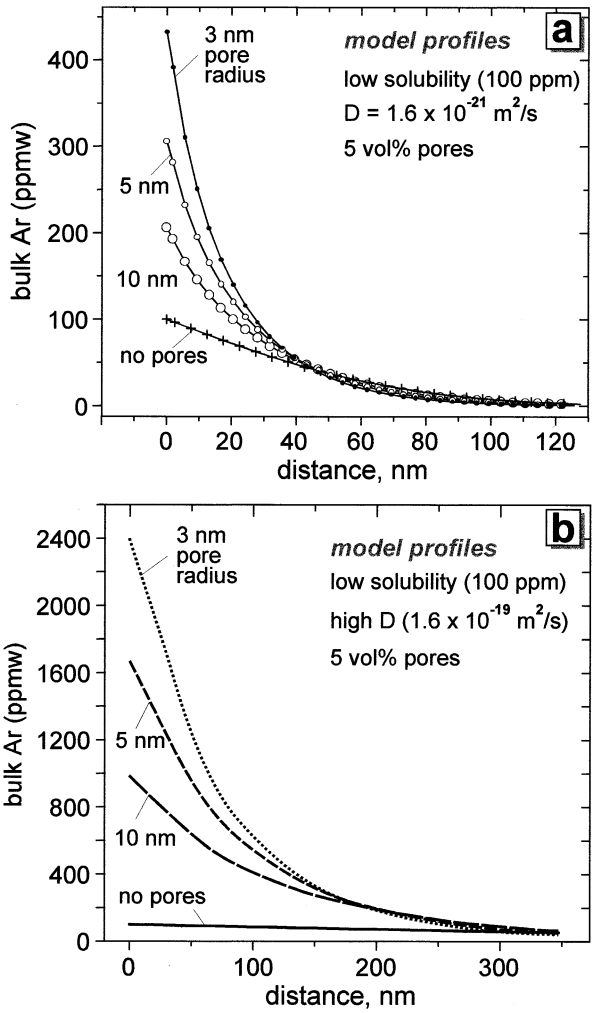

Fig. 13. (a) Bulk Ar-uptake profiles in 5% porous quartz that would result from a low Ar solubility (100 ppm) combined with the low lattice diffusivity measured in this study. When the Ar solubility is low, the bulk Ar concentration rises above the RBS detection limit (~200 ppm) only in the outermost ~10 nm or so of the sample. (b) Bulk Ar-uptake profiles in 5% porous quartz that would result from the combination of a low solubility (100 ppm) and a high lattice diffusivity (100 times higher than our estimate). Despite the presence of pores, Ar penetrates deeper into the bulk sample than is observed in our actual experiments. See text for further discussion.

it would barely be detectable by RBS (see Fig. 13a). This result raises the possibility that the lattice solubility is in fact low but the diffusivity is much higher than we have led ourselves to believe. As in the previous case, this hypothesis can be tested numerically. We ran simulations in which diffusion was accelerated by two orders of magnitude while maintaining the 100-ppm solubility. The results, shown in Figure 13b, suggest two conclusions: (1) pores much smaller than 3 nm (or much more abundant than 5%) are required to generate apparent surface concentrations as high as some of our measured values and (2) if the apparent surface concentrations are allowed to rise even to the lower end of our observed range (~2000 ppm), then the penetration distances greatly exceed those observed. In other words, the combination of low solubility and high diffusivity produces results that are inconsistent with our measured depth profiles.

We ran numerous additional simulations beyond those represented in Figures 9 to 13, incorporating Ar partitioning relationships and pore diffusion-field approximations different from those described in the Appendix. The results can differ in detail from those shown but not in terms of the general behavior of the system. The overall conclusions are not fundamentally changed. The insensitivity to the choice of a pore/lattice Ar partitioning relation, for example, is illustrated in Figure 14, which is a comparison of simulation results incorporating two very different descriptions of Ar partitioning. As discussed in the Appendix, most of the simulations were run assuming a square-root dependence of Ar solubility on Ar pressure, because this is consistent with the limited experimental constraints we have (see Fig. 8) and also because it is suggestive of the site-saturation effect discussed earlier in section 3.2. There is, admittedly, no theoretical justification for this choice, so the success of the numerical simulations cannot be predicated upon it. The other assumed partitioning relation is linear (see Appendix and Fig. 8). Figure 14 shows that bulk Ar uptake into

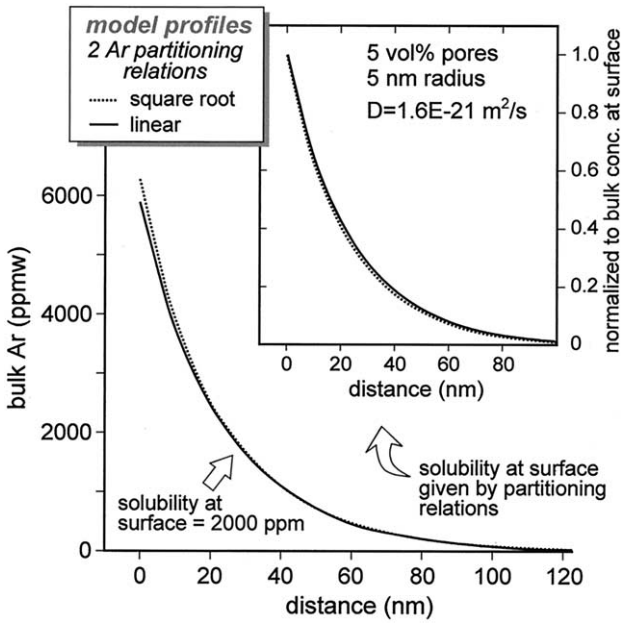

Fig. 14. Results of simulations using two different models for partitioning of Ar between quartz lattice and pores (these are discussed in the Appendix —see Equations A3 and A4—and are illustrated in Fig. 8. In the lower (main) diagram, the lattice concentration at the sample surfaces is taken as 2000 ppm in both cases. In the upper (inset) diagram, the lattice concentration at the sample surfaces is given by the partitioning relation used in the simulations. In this case, the bulk concentrations are normalized to that at the surface to compare the two profiles.

porous quartz is virtually the same for simulations involving the two different partitioning models.

4.2. Diffusion and Solubility Results in the Context of Previous Noble-Gas Studies

4.2.1. Other studies of Ar in quartz

Numerous articles report experimental studies of noble gases in minerals, most of which address either diffusion or solubility (partitioning) but rarely both. The focus of previous studies tends to fall in one of three areas: He in mafic minerals (e.g., Trull and Kurz, 1993), Ar in potassium-bearing minerals (see references in McDougall and Harrison, 1999), or noble-gas partitioning in situations relevant to mantle melting and basalt production in general (e.g., Hiyagon and Ozima, 1982, 1986; Broadhurst et al., 1990, 1992; Brooker et al., 1998; Chamorro et al., 2002). As noted in the "Introduction", however, there also exists a recent study of Ar in quartz. Roselieb et al. (1997) pretreated quartz powders (11–20 μm to 60–80 μm grain size) in pure Ar at 1300 °C and pressures up to 800 MPa and monitored the bulk Ar release characteristics of these samples upon reheating to 1620 °C at 10 °C/min. Their overall conclusion was that the solubility of Ar in quartz is low (30 ppm at most) and that the bulk diffusivity—including contributions from high-diffusivity paths—is high. They acknowledged that diffusion may be slow ($D < 10^{-18}$ m^2/s) outside of structural defects (i.e., in the quartz lattice). Roselieb et al. (1997) examined many of their samples with the EMP and SEM and noted local Ar enrichment to values as high as 4000 ppm, which is consistent with our observation of generally high Ar levels in the near-surface region of all samples exposed to pressurized Ar. High levels would also be expected in localized regions far removed from the crystal surface, provided these had access to the surface via a high-diffusivity pathway. It should be emphasized that the objectives of our study and that of Roselieb et al. (1997) were quite different, so it is not surprising that there are some differences in the findings despite the broad similarities. Our interest was in Ar diffusion in the quartz lattice specifically, because this controls uptake and release of Ar from any defect-free domains in the crystal, whatever the size of these domains. Roselieb et al. (1997), on the other hand, were concerned with bulk-crystal Ar transport, including the role played by high-diffusivity pathways—such as subgrain boundaries and dislocations—that may allow Ar exchange between the crystal interior and the crystal surroundings. Their bulk-uptake/loss approach was well suited to their objectives, while our depth-profiling strategy was required to characterize lattice diffusion outside of any structural defects that might be present.

The only seemingly irreconcilable difference between our conclusions and those of Roselieb et al. (1997) is the solubility of Ar in the quartz lattice. We have discussed our direct and inferential evidence for high solubility at some length, so that all we can do at this point is offer a possible explanation for the difference between their apparent maximum solubility of 30 ppm and our apparent value of ~2000 ppm. If our lattice diffusivity estimates are correct as given by Eqn. 2, then the value at 1300 °C, where the Ar pretreatment runs of Roselieb et al. (1997) were performed, is 1.6×10^{-20} m^2/s. This translates into a characteristic diffusive transport distance, $\sqrt{D \cdot t}$, of only ~130 nm even in the longest pretreatments (12 d) used in the Roselieb et al. (1997) study. Even if structural defects provided "fast-path" diffusive access to the interiors of their quartz grains, the size of lattice domains free of defects would have to be significantly smaller than the 130-nm-length scale for the grains to become fully argonated during pretreatment. If Eqn. 2 is an accurate representation of lattice diffusion, then defect-free lattice domains larger than a few tens of nm would not become saturated with Ar, and, consequently, the solubility would be underestimated by the subsequent bulk Ar release spectra. The patterns would still exhibit the characteristic bimodal distribution of Ar release with increasing temperature that was consistently observed (and logically explained) by Roselieb et al. (1997), the low-temperature peak due to degassing of surfaces and defects—perhaps including the 1.4-nm surface layer identified by Schegel et al. (2002)—and the high-temperature release to degassing of the lattice. This explanation seems consistent with both our data and those of Roselieb et al. (1997), but true reconciliation of the two sets of results will require a better understanding of the defect structure of individual populations of quartz crystals. As in the case of K-feldspar—a mineral well known for its domain-controlled bulk diffusion behavior (McDougall and Harrison, 1999)—exchange of Ar between a quartz crystal and its surroundings is affected at some length scale by lattice diffusion, even if high-diffusivity pathways reduce that length scale to domains much smaller than the crystal size.

4.2.2. Does a structurally anomalous near-surface layer affect our results?

In the preceding section, we concurred with Roselieb et al. (1997) that incorporation (adsorption?) of Ar on or in the quartz surface might affect Ar release spectra for quartz powders. This raises the inevitable question: Do our diffusion and solubility data reflect Ar behavior in some structurally anomalous near-surface region of the quartz crystals rather than in the "normal" lattice? This subject was touched on in the discussion of our zero-time experiments, but it warrants a brief recap at this point. The arguments against the view that our diffusion profiles are confined to a structurally anomalous near-surface layer are as follows:

1. Recent investigations of the near-surface atomic structure of minerals using X-ray reflectivity show that structural perturbations characterized by small relaxations of atoms from their normal positions extend no more than 1 to 1.5 nm into the crystal. All minerals investigated to date (quartz, orthoclase, muscovite, corundum, rutile, calcite, and barite) lead to the same conclusion: only the outermost two or three monolayers are structurally distinct from the normal lattice (Eng et al., 2000; Fenter et al., 2000, 2001; Cheng et al., 2001; N. Sturchio, pers. comm. 2002). In the case of quartz specifically, atom relaxations from normal sites occur no deeper than 1.4 nm (Schlegel et al., 2002). The depths to which Ar penetrates by diffusion into our quartz specimens, although small compared with overall crystal size, are roughly two orders of magnitude greater than the thickness of the structurally anomalous near-surface region.
2. Our diffusion results are consistent and reproducible (within significant uncertainty) irrespective of sample identity, surface treatment, sample preannealing history, or experiment duration (see section 2.2.2). The insensitivity of the data to sample characteristics and pretreatment confirms that the observed uptake of Ar is not due to incorporation of the gas into a damaged or otherwise anomalous near-surface region, because the nature of such a layer would depend on factors that were deliberately varied. The insensitivity to experiment duration confirms that our in-diffusion profiles do not result from rapid penetration into a structurally anomalous region followed by slowing or cessation of diffusion. Out-diffusion of Ar is governed by the same diffusivity as in-diffusion.

4.2.3. Other noble gases in silica polymorphs

Barrer and Vaughn (1967) made a thorough study of He and Ne solubility and diffusion in tridymite and cristobalite using an approach similar to that employed by Roselieb et al. (1997), i.e., bulk uptake of gas into small crystals followed by characterization of the rate of out-gassing upon heating. The diffusivities of He and Ne in tridymite and cristobalite were sufficiently fast and the crystals sufficiently small (~8 μm diameter) that pre-equilibration was assured in most experiments (the authors attempted similar experiments with He in quartz but were unsuccessful due to low solubility or sluggish diffusion or both). The crystal structures and the identity of the noble gases in Barrer and Vaughn (1967) differ from those of the present work, but a comparison of results is tempting and

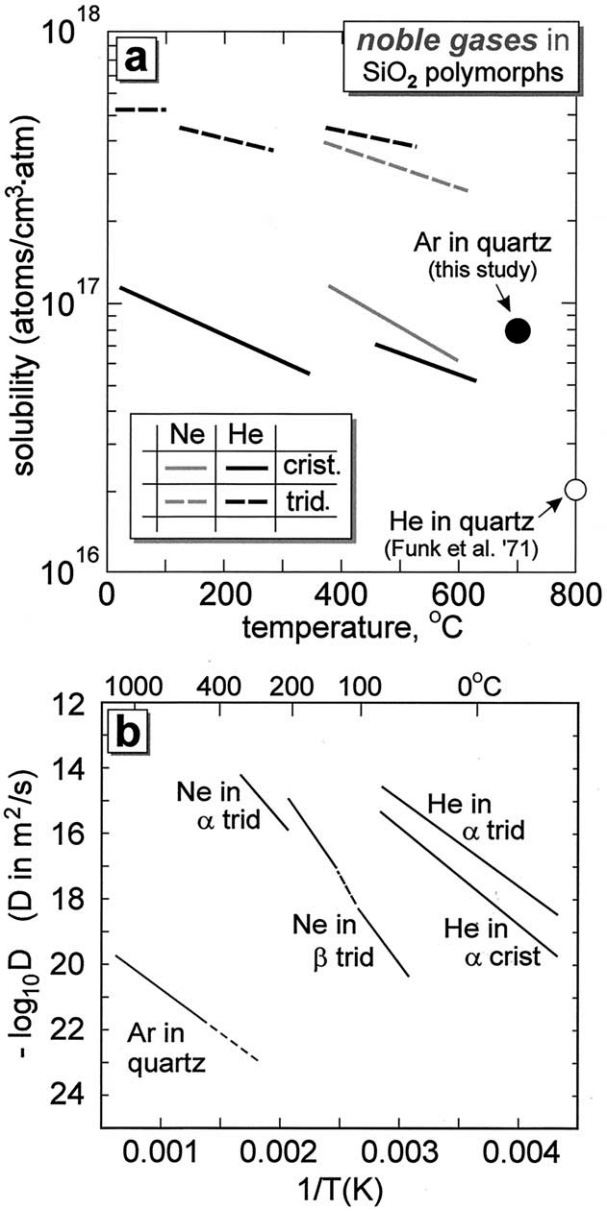

Fig. 15. Solubility and diffusion systematics of He and Ne in tridymite and cristobalite (Barrer and Vaughn, 1967) and quartz (Funk et al., 1971) compared with the present results for Ar in quartz. Funk et al. (1971) also characterized relative diffusivities for He in quartz at various temperatures but did not assign absolute values (see text).

the systematics are interesting. As shown in Figure 15a, our best-guess solubility of Ar in quartz at ~700 °C is similar to that of He and Ne in cristobalite at somewhat lower temperatures (He and Ne are more soluble in tridymite than in cristobalite by a factor of 6 to 8). Barrer and Vaughn (1967) observed no tendency for He and Ne to saturate available sites at pressures up to ~80 MPa (recall that quartz may saturate in Ar at 50 to 100 MPa; see Fig. 8). Funk et al. (1971) examined He solubility and diffusion in quartz using an approach like that of Barrer and Vaughn (1967) involving bulk uptake followed by out-gassing. The reported solubility of He is a factor of ~4 lower than our apparent value for Ar (see Fig. 15a).

Data on diffusion of noble gases in the silica polymorphs are summarized in Figure 15b; unfortunately, Barrer and Vaughn (1967) were unable to obtain diffusivity data for Ne in cristobalite because diffusion was too sluggish. Again, because of differences in diffusant atoms and host crystal structures, there is no expectation that robust correlations or fundamental truths will emerge from the comparison. However, it can be concluded from this diagram that our low measured diffusivities for Ar in quartz are reasonable and consistent with other data. To appreciate the reasoning, it is helpful to know that the densities of quartz, cristobalite, and tridymite are 2.65, 2.33, and 2.26 g/cm^3, respectively. These values imply a ranking of structural openness (or, quantitatively, ionic porosity; see Dowty, 1980; Fortier and Giletti, 1989) in the order tridymite $>$ cristobalite $>$ quartz. It is useful to know also that Ne and Ar atoms are $\sim$20 and 70% larger, respectively, than He atoms (e.g., Pauling, 1927; Bondi, 1964). Given these statistics, the observed slow diffusion of Ne relative to He in the polymorphs studied by Barrer and Vaughn (1967) is reasonable, simply because of the difference in size of the atoms. If data for Ar diffusion in tridymite were available, the Arrhenius line would logically fall orders of magnitude below that for Ne because the Ar atom is much larger. The tighter structure of quartz relative to the other polymorphs implies still lower diffusivities for this mineral—a prediction not inconsistent with our data. Citing concern over possible low-temperature He loss, Funk et al. (1971) declined to put absolute values on the diffusivity of He in quartz, commenting only that He diffusion appeared to be at least two order[s] of magnitude lower than expected for quartz based on a comparison with the data of Barrer and Vaughn (1967). The activation energy was determined to be 54 to 65 kJ/mol.

The one puzzling aspect of Figure 15b is that our 51 kJ/mol activation energy for Ar diffusion in quartz is so low (it is comparable, in fact, with that for He diffusion in tridymite, cristobalite, and quartz). As noted previously, the scatter in our data at any given temperature is large because of the inherent challenges in the analysis (see sections 3.2 and 4.1). Nevertheless, the large (700 °C) temperature range covered by our data constrains the activation energy reasonably well. It should be noted that while the vast majority of our data apply to β-quartz (stable above $\sim$600 °C at 100 MPa), the six values at T $<$ 600 °C actually pertain to α-quartz; these do exert some leverage in the least-squares fit that determines the activation energy. Technically speaking, the data above and below $\sim$600 °C do not belong on the same Arrhenius line, but fitting separate lines is unwarranted because of imprecision in the data and also because a single polymorph (β-quartz) was stable over most of the temperature range we investigated (i.e., a full 600—1200 °C). Barrer and Vaughn (1967) did observe slightly different diffusion behavior for Ne in α and β forms of tridymite (see Fig. 15b). Fortunately, in applying our diffusion data to natural systems, the somewhat uncertain temperature dependence of Ar diffusion in quartz should not be too devastating, because our data cover much of the range of geologic interest, and they apply to the forms of quartz that are present in nature. Long extrapolations based on a somewhat uncertain activation energy will seldom if ever be necessary.

4.3. Concluding Remarks: Geochemical Applications and Implications

From this study emerge a few relatively firm conclusions about the behavior of Ar in the Earth's crust, along with numerous possible speculations and avenues for future research. On the more substantive side, it seems clear that quartz can incorporate significant amounts of Ar under optimal circumstances of saturation with respect to pure, pressurized Ar gas. This does not mean that Ar is compatible in quartz in a trace-element-partitioning sense. On the contrary, the quartz/gas partition coefficient, expressed using conventional units for noble-gas partitioning between condensed phases and gas (Ozima and Podosek, 2002), is only $\sim$0.001 cm^{3}STP/g $\cdot$ atm. The solubility measurements are not directly relevant to any natural situation. We note, however, that the 1-GPa experiments involving organic clathrate as the Ar source do in fact represent Ar partitioning between quartz and C-O-H fluid; significant amounts of Ar entered the quartz lattice under these circumstances (see Table 1). These results are qualitative because the exact composition and amount of fluid is not known, but they do confirm uptake of some Ar into quartz coexisting with fluid containing several wt.% Ar. More favorable partitioning into quartz might occur when quartz coexists with rhyolite melt. Our best-guess solubility value for Ar in quartz ($\sim$2000 ppm at 100 MPa; see Figs. 4, 8, and 9b) can be divided by the solubility of Ar in rhyolite melt given by Carroll and Draper (1994). Ignoring differences in temperature (and the fact that natural melts would contain dissolved water), the resulting quartz/rhyolite partition coefficient for Ar is $\sim$3. Although probably not quantitatively correct, this value does suggest somewhat compatible behavior of Ar in quartz relative to melt in felsic magmas.

The ability of quartz to accommodate Ar under some conditions makes this mineral a potentially significant sink for Ar in the crust. Viewed one way, this conclusion is not very profound, because the rate of ^{40}Ar production even in pure potassium feldspar is only $\sim$1 ppb/Ma, so the storage requirements are modest in absolute terms. It should be acknowledged, also, that even if Ar could not be stored in the quartz lattice specifically, micro- or nano-scale fluid inclusions may serve as minute reservoirs for Ar, as demonstrated in this study and also by Kelley et al. (1986). What is interesting about the new results is that Ar may actually be partitioned into the quartz lattice relative to other phases in a natural system. This possibility was put forth by Baxter et al. (2002) as a possible explanation for differences in Ar behavior in (quartz-rich) pelites relative to adjacent (quartz-poor) amphibolites near Simplon Pass, Switzerland. At present, our sense is that Ar partitions into quartz to a significant extent in systems lacking a free vapor phase. However, the presence of C-O-H fluid would change the picture dramatically—such a phase would serve as the principal host and transport medium for Ar. The role and properties of a hypothetical, structurally undefined intergranular or grain-boundary region (see, e.g., Brady, 1983) remain uncertain.

An additional, quite interesting aspect of our Ar diffusion data is that they allow open-system behavior of Ar with respect to quartz at low temperatures, as required by the Baxter et al. (2002) model. The data provide a general explanation for why,

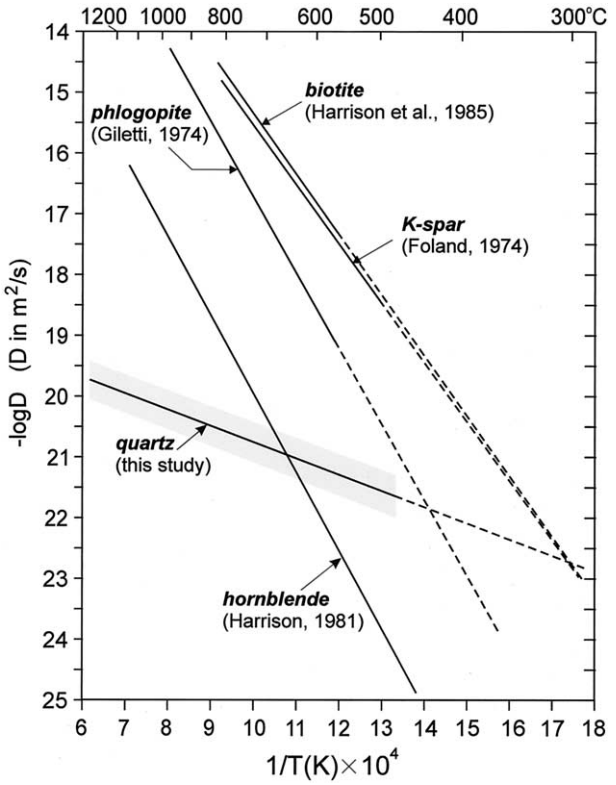

Fig. 16. Arrhenius diagram summarizing laboratory-determined Ar diffusion characteristics of several K-bearing minerals in comparison with the new data for quartz. The Arrhenius lines are solid over the range of temperature where experimental data were obtained; the dashed lines are extrapolations. The shaded region for quartz is the 2σ confidence band (see Fig. 3).

if Ar is (as we suggest) somewhat compatible in quartz under fluid-absent conditions, high concentrations are rarely documented in quartz separates: Ar may remain sufficiently mobile to diffuse out of the quartz lattice even at upper crustal conditions. This point is underscored in Figure 16, which is a selective summary of Ar diffusion behavior in several K-bearing minerals (micas, hornblende, K-spar) relative to quartz. Diffusion in micas and homogeneous orthoclase is faster than in quartz at temperatures above 300 to 500 °C, but the low activation energy for Ar diffusion in quartz leads to higher diffusivities in this mineral at low temperatures.

Significant compatibility of noble gases—or at least the lack of total incompatibility—has been suggested for a number of minerals besides quartz. Anorthite, diopside, forsterite, and spinel have all been shown to incorporate not only Ar but also Kr and Xe (Broadhurst et al., 1990, 1992) in concentrations subequal to or higher than those in coexisting haplobasaltic melts. In part because of the substantial uncertainties in the data, the Broadhurst et al. (1990, 1992) results are controversial (see, e.g., Carroll and Draper, 1994; Chamorro et al., 2002; Ozima and Podosek, 2002, p. 54), and it is uncertain whether the noble gases resided in the mineral lattices or in defects. The new data indicating significant Ar solubility in quartz certainly cannot be generalized to all noble gases and all minerals, but it seems possible that some silicates are better hosts for noble gases than has generally been assumed. Even in a pure oxide of very simple structure such as periclase (MgO), noble gases can be accommodated in the lattice in one of three ways (see Tsuchiyama and Kawamura, 1994): interstitial, unassociated vacancy (e.g., replacing a missing cation or anion only), and associated vacancy (replacing a missing cation–anion pair). The theoretical treatment of Tsuchiyama and Kawamura (1994) does not make predictions of Ar partitioning into MgO relative to other phases, but our preliminary results indicate RBS-detectable levels of Ar in MgO subjected to pressurized Ar (~600–800 °C, 50–200 MPa).

The demonstrated sporadic involvement of nanopores in the intragrain behavior of Ar in laboratory samples underscores the probable complexities of noble-gas behavior in minerals in their natural settings. Rock-forming minerals are known to be porous on many scales (e.g., Montgomery and Brace, 1975; Parsons et al., 1988; David and Walker, 1990; Worden et al., 1990; Brantley and Mellott, 2000). If the porosity is interconnected, it is reasonable to expect enhanced bulk-crystal transport of gas atoms (see, e.g., David and Walker, 1990); interestingly, the nanopores in the quartz crystals we examined (Fig. 7) are isolated from one another and, in consequence, actually have a minor inhibiting effect on the rate and length scale of bulk-crystal Ar diffusion, along with an occasionally dramatic enhancing effect on apparent lattice solubility. The same general tendencies could arise in nature when small fluid inclusions are present.

Additional experimental data for both solubility and diffusion of noble gases in all geologically relevant minerals are highly desirable. The direct profiling method may be the best way to obtain such data—or at least a powerful complement to the bulk outgassing approach—in cases where the solubility and diffusivity fall in a range that makes them accessible to existing depth-profiling technologies. We are by no means the first to advocate this view: Carroll and Stolper (1991) took advantage of a high diffusivity and solubility to complete a study of Ar in SiO_2 glass using an experimental protocol very similar to the present one, in which enviably long diffusion profiles were characterized by EMP (supplemented by RBS). Wartho et al. (1999) have pioneered the use of UV laser ablation depth profiling to examine Ar diffusion in potassium feldspar. The advantage of their analytical technique over ours is a much lower detection limit for Ar; however, laser ablation does not have the depth resolution obtainable by RBS, and as this study has shown, the outermost 100 nm of a crystal may contain crucial information about gas uptake in some cases. A potentially important goal of future research efforts along the lines of this study is to establish a correlation between noble gas solubilities and the local defect structure of individual minerals.

Acknowledgments—We thank Jun Abrajano (mass-spec analysis of Ar gas), Ray Dove (field-emission SEM), Bob Hepburn (FTIR), Dave Wark (EMP and SEM), and Neil Sturchio (mineral surface structure) for their help and guidance during the course of this study. Jason Bender and Yulia Frenkel provided assistance in the lab during our efforts to capture Ar in hydroquinone. Ethan Baxter kindly provided a draft of the Baxter et al. (2002) manuscript and later contributed valuable comments on an early draft of this paper. The official review comments of Simon Kelley, Knut Roselieb, and an anonymous reviewer led to additional confirmatory experiments and extensive revision of the original manuscript. The research leading to this paper was supported by the National Science Foundation under grant no. EAR-9804794.

Associate editor: M. Harrison

REFERENCES

Aines R. D. and Rossman G. R. (1984) Water in minerals? A peak in the infrared. *J. Geophys. Res.* **89,** 4059–4071.

Aines R. D. and Rossman G. R. (1985) The high-temperature behavior of trace hydrous components in silicate minerals. *Am. Mineral.* **70,** 1169–1179.

Barrer R. M. and Vaughn D. E. W. (1967) Solution and diffusion of He and Ne in tridymite and cristobalite. *Trans. Faraday Soc.* **63,** 2275–2290.

Baxter E. F., DePaolo D. J., and Renne P. R. (2002) Spatially correlated anomalous 40Ar/39Ar "age" variations in biotites about a lithologic contact near Simplon Pass, Switzerland: A mechanistic explanation for excess Ar. *Geochim. Cosmochim. Acta* **66,** 1067–1084.

Bondi A. (1964) Van der Waals volumes and radii. *J. Phys. Chem.* **68,** 441–451.

Brady J. B. (1983) Intergranular diffusion in metamorphic rocks. *Am. J. Sci.* **283,** 181–200.

Brantley S. L. and Mellott N. P. (2000) Surface area and porosity of primary silicate minerals. *Am. Mineral.* **85,** 1767–1783.

Broadhurst C. L., Drake M. J., Hagee B. E., and Bernatowitz T. J. (1990) Solubility and partitioning of Ar in anorthite, diopside, forsterite, spinel, and synthetic basaltic liquids. *Geochim. Cosmochim. Acta* **54,** 299–309.

Broadhurst C. L., Drake M. J., Hagee B. E., and Bernatowitz T. J. (1992) Solubility and partitioning of Ne, Ar, Kr, and Xe in minerals and synthetic basaltic melts. *Geochim. Cosmochim. Acta* **56,** 709–723.

Brooker J. A., Wartho J.-A., Carroll M. R., Kelley S. P., and Draper D. S. (1998) Preliminary UVLAMP determinations of argon partition coefficients for olivine and clinopyroxene grown from silicate melts. *Chem. Geol.* **147,** 185–200.

Carroll M. R. and Draper D. S. (1994) Noble gases as trace elements in magmatic processes. *Chem. Geol.* **117,** 37–56.

Carroll M. R. and Stolper E. M. (1991) Argon solubility and diffusion in silica glass: Implications for the solution behavior of molecular gases. *Geochim. Cosmochim. Acta* **55,** 211–225.

Chamorro E. M., Brooker R. A., Wartho J.-A., Wood B. J., Kelley S. P., and Blundy J. D. (2002) Ar and K partitioning between clinopyroxene and silicate melt to 8 GPa. *Geochim. Cosmochim. Acta* **66,** 507–519.

Cheng L., Fenter P., Nagy K., Schlegel M., and Sturchio N. C. (2001) Molecular scale density oscillations in water adjacent to a mica surface. *Phys. Rev. Lett.* **87,** 56103–1 –56103-4.

Cherniak D. J. (1995) Diffusion of lead in plagioclase and K-feldspar: An investigation using Rutherford backscattering and resonant nuclear reaction analysis. *Contrib. Mineral. Petrol.* **120,** 358–371.

Cherniak D. J. and Watson E. B. (1992) a study of strontium diffusion in K-feldspar, Na-K feldspar and anorthite using Rutherford backscattering spectroscopy. *Earth Planet. Sci. Lett.* **113,** 411–425.

Chu W.-K., Meyer J. W., and Nicolet M.-A.(1978) *Backscattering Spectrometry.* Academic Press, New York.

Crank J. (1975) *The Mathematics of Diffusion*. 2nd ed. Oxford University Press, New York.

Cumbest R. J., Johnson E. L., and Onstott T. C. (1994) Argon composition of metamorphic fluids: Implications for $^{40}Ar/^{39}Ar$ geochronology. *Geol. Soc. Am. Bull.* **106,** 942–951.

Cussler E. L. (1997) *Diffusion: Mass Transfer in Fluid Systems*. 2nd ed. Cambridge University Press, New York.

David F. and Walker L. (1990) Ion microprobe study of intragrain micropermeability in alkali feldspars. *Contrib. Mineral. Petrol.* **106,** 124–128.

Doremus R. H. (2002) *Diffusion of Reactive Molecules in Solids and Melts*. John Wiley & Sons, New York.

Dowty E. (1980) Crystal-chemical factors affecting the mobility of ions in minerals. *Am. Mineral.* **65,** 174–182.

Eng P. J., Trainor T. P., and Brown G. E. (2000) Structure of the hydrated alpha-Al_2O_3 surface. *Science* **288,** 1029–1033.

Fenter P., Teng H., Geissbuhler P., Nagy K., and Sturchio N. C. (2000) Atomic scale structure of the orthoclase (001)-water interface measured with X-ray reflectivity. *Geochim. Cosmochim. Acta* **64,** 3663–3673.

Fenter P., McBride M. T., Srajer G., Sturchio N. C., and Bosbach D. (2001) Structure of barite(100)- and (210)-water interfaces. *J. Phys. Chem.* **B105,** 8112–8119.

Foland K. A. (1974) ^{40}Ar diffusion in homogeneous orthoclase and an interpretation of Ar diffusion in K-feldspar. *Geochim. Cosmochim. Acta* **38,** 151–166.

Foland K. A. (1979) Limited mobility of Ar in metamorphic terrain. *Geochim. Cosmochim. Acta* **43,** 793–801.

Funk H., Baur H., Frick U., Schultz L., and Signer P. (1971) On the diffusion of He in quartz. *Zeitschrift fur Kristallographie* **133,** 225–233.

Giletti B. J. (1974) Studies in diffusion I: Argon in phlogopite mica. In *Geochemical Transport and Kinetics.* (eds. A. W. Hofmann et al.), pp. 107–115. Carnegie Inst. Wash. Publ. 634.

Greenwood N. N. and Earnshaw A. (1984) *Chemistry of the Elements*. Pergamon Press, New York.

Harrison T. M. (1981) Diffusion of ^{40}Ar in hornblende. *Contrib. Mineral. Petrol.* **78,** 324–331.

Harrison T. M. and McDougall I. (1981) Excess ^{40}Ar in metamorphic rocks from Broken Hill, New South Wales: Implications for $^{40}Ar/^{39}Ar$ age spectra and the thermal history of the region. *Earth Planet. Sci. Lett.* **55,** 123–149.

Harrison T. M., Duncan I., and McDougall I. (1985) Diffusion of ^{40}Ar in biotite: Temperature, pressure and compositional effects. *Geochim. Cosmochim. Acta* **49,** 2461–2468.

Hiyagon H. and Ozima M. (1982) Noble gas distribution between basalt melt and crystals. *Earth Planet. Sci. Lett.* **58,** 255–264.

Hiyagon H. and Ozima M. (1986) Partition of noble gases between olivine and basaltic melt. *Geochim. Cosmochim. Acta* **50,** 2045–2057.

Holloway J. R. (1977) Fugacity and activity of molecular species in super-critical fluids. In *Thermodynamics in Geology* (ed. D. G. Fraser), pp. 161–181, D. Reidel, Boston.

Kelley S. P. and Wartho J.-A. (2000) Rapid kimberlite ascent and the significance of Ar-Ar ages in xenolith phlogopites. *Science* **289,** 609–611.

Kelley S. P., Turner G., Butterfield A. W., and Shepherd T. J. (1986) The source and significance of argon isotopes in fluid inclusions from areas of mineralization. *Earth Planet. Sci. Lett.* **79,** 303–318.

Laughlin A. W. and Yoder H. S. (1971) Introduction and diffusion of argon into natural albite. *Carnegie Inst. Wash. Yrbk.* **69,** 145–148.

McDougall I. and Harrison T. M. (1999) *Geochronology and Thermochronology by the $^{40}Ar/^{39}Ar$ Method*. Oxford University Press, New York.

Montgomery C. W. and Brace W. F. (1975) Micropores in plagioclase. *Contrib. Mineral. Petrol.* **52,** 17–28.

Ozima M. and Podosek F. A. (2002) *Noble Gas Geochemistry*, 2nd ed. Cambridge University Press.

Parsons I., Rex D. C., Guise P., and Halliday A. N. (1988) Argon-loss by alkali feldspars. *Geochim. Cosmochim. Acta* **52,** 1097–1112.

Pauling L. (1927) The sizes of ions and the structure of ionic crystals. *J. Am. Chem. Soc.* **49,** 765–790.

Roddick J. C., Cliff R. A., and Rex D. C. (1980) The evolution of excess argon in alpine biotites—a $^{40}Ar/^{39}Ar$ analysis. *Earth Planet. Sci. Lett.* **48,** 185–208.

Roedder E. (1984) *Fluid Inclusions*. *Reviews in Mineralogy*, Vol. 12 (ed. P. H. Ribbe), pp. 70 ff,264 ff. Mineralogical Society of America, Washington, D.C.

Roselieb K., Blanc P., Büttner H., Jambon A., Rammensee W., Rosenhauer M., Vielzeuf D., and Walter H. (1997) Experimental study of argon sorption in quartz: Evidence for argon incompatibility. *Geochim. Cosmochim. Acta* **61,** 533–542.

Scaillet S. (1996) Excess ^{40}Ar transport scale and mechanism in high-pressure phengites: A case study for eclogitized metabasite of the Dora-Maira nappe, western Alps. *Geochim. Cosmochim. Acta* **60,** 1075–1090.

Schlegel M. L., Nagy K. L., Fenter P., and Sturchio N. (2002) Structures of quartz (1010)- and (1010)-water interfaces determined by X-ray reflectivity and atomic force microscopy of natural growth surfaces. *Geochim. Cosmochim. Acta* **66,** 3037–3054.

Trull T. W. and Kurz M. D. (1993) Experimental measurements of ^{3}He and ^{4}He mobility in olivine and clinopyroxene at magmatic temperatures. *Geochim. Cosmochim. Acta* **57,** 1313–1324.

Tsuchiyama A. and Kawamura K. (1994) Sites and behaviors of noble gas atoms in MgO crystal simulated by the molecular dynamics (MD) method. In *Nobel Gas Geochemistry and Cosmochemistry* (ed. J. Matsuda), pp. 315–323. Terra Scientific Publishing, Tokyo.

Wartho J.-A., Kelley S. P., Brooker R. A., Carroll M. R., Villa I. M., and Lee M. R. (1999) Direct measurement of Ar diffusion profiles in a gem-quality Madagascar K-feldspar using the ultra-violet laser ablation microprobe. *Earth Planet. Sci. Lett.* **170,** 141–153.

Watson E. B. and Cherniak D. J. (1997) Oxygen diffusion in zircon. *Earth Planet. Sci. Lett.* **148,** 527–544.

Worden R. H., Walker F. D. L., Parsons I., and Brown W. L. (1990) Development of microporosity, diffusion channels and deuteric coarsening in perthitic alkali feldspars. *Contrib. Mineral. Petrol.* **104,** 507–515.

York D. (1969) Least-squares fitting of a straight line with correlated errors. *Earth Planet. Sci. Lett.* **5,** 320–324.

Zhang Y., Stolper E. M., and Wasserburg G. J. (1991) Diffusion of a multi-species component and its role in oxygen and water transport in silicates. *Earth Planet. Sci. Lett.* **103,** 228–240.

APPENDIX

To strengthen the pore interpretation of the high-Ar diffusive uptake profiles, we undertook numerical simulations of diffusion in a lattice that is sparsely populated by pores. Argon diffusion into a quartz lattice sparsely populated by pores can be visualized as one-dimensional diffusion into a semi-infinite medium containing local "sinks" for the diffusant. The time dependence of the local concentration of Ar is described by the non-steady-state diffusion equation with an added sink term:

$$\frac{\partial C_q}{\partial t} = D\,\frac{\partial^2 C_q}{\partial X^2} - \frac{\partial S}{\partial t} \qquad \text{(A1)}$$

where C_q is concentration, X is distance, and S represents concentration in a local sink (an equation of this form applies, for example, to diffusion accompanied by an immobilizing reaction or "trap" (see, e.g., Crank, 1975; Cussler, 1997; Doremus, 2002). Our Ar-in-quartz problem is complicated by the fact that the pores are sparse—hence many Ar atoms do not encounter pores on their way through the quartz lattice—and also because Ar fills the pores at a rate that is neither constant nor linear in time. The pore filling is controlled by diffusion in a local field surrounding each pore and also by partitioning of Ar between the pores and the quartz lattice. Moreover, since Ar diffusion in quartz is slow, the scale of bulk transport does not vastly exceed the scale of the pores. A three-dimensional finite-element simulation would be required to map in detail the distribution of Ar as it diffuses into slightly porous quartz under these circumstances. However, the general characteristics of the diffusion process can be recovered with a simpler approach. We chose to account for local diffusion of Ar into a given pore with the following approximation:

$$\frac{\mathrm{d}n_p}{\mathrm{d}t} = -D\,\frac{(C_w - C_q)}{\sqrt{D\cdot\tau}}\cdot A_p \qquad \text{(A2)}$$

where n_p is the number of Ar atoms in the pore, A_p is the pore surface area, C_w is the concentration (moles Ar per cm^3) of Ar in quartz at the pore wall, and C_q is the concentration of Ar in quartz just beyond the local diffusion field around the pore (i.e., the "regional" concentration). The $\sqrt{D\cdot\tau}$ term in the denominator is a local diffusion length scale in which τ is the time elapsed since C_q exceeded zero for the pore under consideration. This term approximates the width of the diffusion field around the pore, so $(C_w - C_q)/\sqrt{D\cdot\tau}$ is the local concentration gradient driving diffusion into the pore. A schematic representation of the bulk diffusion model and the parameters discussed above is shown in Figure A1.

The concentration of Ar in quartz at the pore wall, C_w, is determined by partitioning equilibrium with the gas in the pore. The partitioning relationship is not exactly known, but we extracted an approximate one from our apparent solubility data (Fig. 8), assuming that our lowest values at ~12, 20, and 100 MPa represent the actual solubility of Ar in the quartz lattice. This relationship is

$$C_w = 0.00115\cdot C_p^{1/2} \qquad \text{(A3)}$$

where C_p is Ar concentration in the pore and both concentrations are expressed as moles of Ar per cm^3 of material (the molar volume of Ar gas at the pressure of interest was calculated from the Redlich-Kwong equation as described in Holloway, 1977). A curve corresponding to Eqn. A3 is shown on Figure 8. Note that this relation gives a solubility at 100 MPa similar to that suggested by Figure 9b.

Because the Ar partitioning relation in Eqn. A3 is not well constrained, it is important to show that the model results are not sensitive to this choice. For this reason, we also ran simulations using a significantly shallower, linear dependence of solubility on pressure (i.e., on gas density) given by

$$C_w = 0.0053\cdot C_p \qquad \text{(A4)}$$

This relation is shown graphically on Figure 8.

An iterative code was written to simulate the overall process of Ar diffusion into porous quartz using standard explicit finite difference techniques. In a given time step, the change in Ar concentration in each volume element was computed by summing the influx and outflow due to the regional concentration gradient and the loss due to diffusion into the local pores (described by Eqn. A2). Normal precautions to insure stability were taken (see, e.g., Crank 1975), and the resulting regional profiles were integrated to test for conservation of Ar during each simulation.

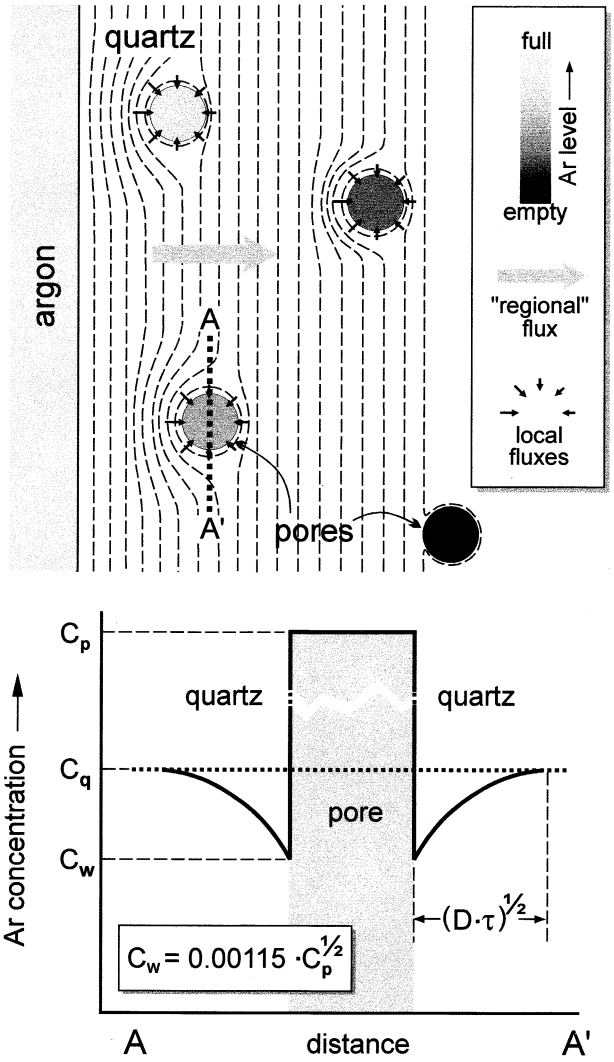

Fig A1. Schematic representation of diffusion from a planar surface (at the left in the top diagram) into a medium sparsely populated by pores. The overall regional flux into the bulk medium is indicated by the large gray arrow and the local fluxes into the pores by small black arrows. Dashed lines are hypothetical isoconcentration contours. The pores gradually fill with Ar as ndicated by the grayscale bar. A schematic concentration profile (A-A′) in the region of a single pore is shown in the bottom panel with model parameters indicated. See text of Appendix for details.